Check for updates

Meteorological Applications

RMetS Royal Meteorological Society

RESEARCH ARTICLE OPEN ACCESS

Improving Land Surface Model Soil Moisture Estimates Through Joint State-Parameter Assimilation of In Situ Soil Moisture Observations

Ramesh Visweshwaran[1,2] | Elizabeth Cooper[3] | Sarah L. Dance[1,2,4]

[1]Department of Meteorology, University of Reading, Reading, UK | [2]National Centre for Earth Observation (NCEO), University of Reading, Reading, UK | [3]UK Centre for Ecology & Hydrology (UKCEH), Wallingford, UK | [4]Department of Mathematics & Statistics, University of Reading, Reading, UK

Correspondence: Ramesh Visweshwaran (v.ramesh@reading.ac.uk)

Received: 21 March 2026 | **Revised:** 14 September 2026 | **Accepted:** 24 September 2026

Keywords: COSMOS-UK | data assimilation | En-Var | JULES | pedotransfer function | soil moisture | state-parameter estimation

ABSTRACT

Accurate soil moisture estimates are essential for effective management and operational planning of flood and drought events, both of which are intensifying under a changing climate. However, soil moisture values derived from land surface models often exhibit significant deviations from in situ observations. Data assimilation combines model information with observations to enhance prediction accuracy. Previous studies have typically focused on either estimating the initial soil moisture state or optimising Pedotransfer Function (PTF) constants (or parameters), which link soil texture to the hydraulic properties of land surface models. In contrast, this study introduces a novel extension by performing joint state-parameter assimilation for the JULES model, simultaneously optimising both PTF constants and initial soil moisture states within an augmented framework. Using an Ensemble–Variational hybrid data assimilation scheme, we ingested field-scale soil moisture observations from the Cosmic-ray Soil Moisture Monitoring Network across 16 diverse sites in the UK. The joint state-parameter assimilation improved average Kling–Gupta Efficiency by approximately 113% relative to the open-loop, 105% relative to state-only and 9.6% relative to parameter-only experiments. These results highlight the strong potential of the proposed framework for enhancing land-surface reanalysis, numerical weather prediction and hydrometeorological forecasting of floods and droughts.

1 | Introduction

Soil moisture plays a significant role in land surface processes due to its strong influence on various components of the water cycle (Huggannavar and Indu 2020). Consequently, accurate representation of soil moisture is crucial for water resource management, irrigation scheduling and flood and drought responses. Reliable soil moisture estimates also support land-surface reanalysis, enhancing numerical weather prediction and informing long-term climate assessments (Visweshwaran, Ramsankaran, Eldho, and Jha 2022; Subbarayan et al. 2025; Hou and Pu 2023; Brocca et al. 2017; Visweshwaran et al. 2024).

Land surface models (LSMs) can estimate soil moisture conditions at various soil depths and across a range of spatial and temporal scales. However, these estimates are uncertain. The uncertainties can stem from errors in the forcing variables, such as rainfall and temperature data, and the model's inherent structural limitations, including parameter inaccuracies and improper initialisation of the soil moisture conditions

This is an open access article under the terms of the Creative Commons Attribution License, which permits use, distribution and reproduction in any medium, provided the original work is properly cited.

© 2026 The Author(s). *Meteorological Applications* published by John Wiley & Sons Ltd on behalf of Royal Meteorological Society.

(Alvarado-Montero et al. 2017). In addition, modern LSMs, such as the Joint UK Land Environment Simulator (JULES), rely on empirical soil models or pedotransfer functions (PTFs) like Cosby (Cosby et al. 1984) or Toth models (Tóth et al. 2015) to translate commonly available soil properties like texture into hydraulic parameters (hydraulic conductivity and soil matric suction) essential for running the model. The constants within these PTFs are often derived through statistical regression analyses fitted against soil databases (Van Looy et al. 2017), and thus carry inherent uncertainty that can vary across soil types. Uncertainty resulting from inaccuracies in PTF constants can also propagate through the model, reducing the reliability of model forecasts.

On the other hand, soil moisture can be observed using in situ instruments or remote sensing platforms. Remotely sensed observations such as Soil Moisture and Ocean Salinity (SMOS; Kerr et al. 2001), Soil Moisture Active Passive (SMAP; Entekhabi et al. 2010), Advanced Scatterometer (ASCAT; Wagner et al. 2013), determine soil moisture conditions across a wide area, but provide information only at the surface level due to low penetration capacity (Albergel et al. 2012). Conversely, in situ observations from networks like Aquitaine soil moisture network, France (FR-AQUI; Wigneron et al. 2018), the Center for Western Weather and Water Extremes network (CW3E; Sumargo et al. 2021) and the GROW Observatory (Xaver et al. 2020) provide soil moisture conditions at both surface (0–5 cm) and subsurface levels (up to 100 cm depth). However, these observations are limited to point locations at selected sites, offering less spatial coverage compared to satellite-based methods. In recent years, new approaches have been developed to measure soil moisture at the field scale. The Cosmic-ray Soil Moisture Monitoring Network (COSMOS-UK), provided by the UK Centre for Ecology and Hydrology (UKCEH), uses cosmic ray neutron sensors to monitor soil moisture conditions. These sensors provide volumetric water content estimates over a horizontal footprint of approximately 12 ha and to a vertical depth of up to 80 cm, with a measurement uncertainty of approximately 0.04 $m^3\ m^{-3}$ (Cooper, Bennett, et al. 2021; Stanley et al. 2023).

Given the complementary strengths and limitations of LSMs and observation networks, there is a clear need for a framework that can leverage both. Data assimilation (DA) offers this by optimally combining information from both sources, accounting for their respective uncertainties (Beven and Binley 1992; Kumar et al. 2022; Xu et al. 2025).

In land data assimilation systems, soil moisture assimilation has gained considerable attention (Ramesh et al. 2025; Mason et al. 2020; Tian et al. 2021; Visweshwaran, Ramsankaran, Eldho, and Lakshmivarahan 2022; Heyvaert et al. 2024). Sequential methods (like Ensemble filters) are widely used due to their relatively simple and cost-effective implementation (Cooper et al. 2019; Gong et al. 2024). They dynamically update model states and parameters at frequent intervals, which may not be consistent with the stable (non-chaotic) nature of land surface processes (Shi et al. 2015; Raoult et al. 2025). On the other hand, variational techniques (like 4D-Var) can use a longer assimilation window timeframe and establish time-invariant state-parameter values over the duration of this window (Smith et al. 2013; Pinnington et al. 2017). Due to the high dimensionality and complexity of JULES, along with the frequent release of new versions, calculating the gradient of the dynamical model and the observation operator has become both computationally expensive and inefficient. Hybrid data assimilation methods, such as the Ensemble-Variational (En-Var) approach, combine features of both variational and ensemble techniques by using ensemble-based prior error covariances within a variational framework. En-Var avoids the need to explicitly compute the full model adjoint while still approximating the model trajectory over an assimilation window, offering a flexible alternative to traditional approaches (Lorenc et al. 2015; Poterjoy and Zhang 2015). Other gradient-free statistical approaches, like Markov chain Monte Carlo (MCMC), are often computationally prohibitive for high-dimensional systems, as they require many model realisations to effectively sample the probability density. In contrast, the En-Var approach only requires a moderate ensemble size and enables reusability of model trajectories across experiments. These characteristics make this approach a robust and flexible option for building data assimilation systems for complex LSMs like JULES.

In the context of land surface modelling, data assimilation is used for state estimation in numerical weather prediction (Mahfouf and Viterbo 1996) and land-surface reanalysis systems (Muñoz Sabater et al. 2021), or for parameter estimation where model parameters are optimised to reduce structural errors and improve long-term simulation accuracy. However, the two are rarely performed simultaneously. Previous studies on parameter estimation in LSMs using soil moisture observations have focused on either directly improving the model's soil parameters (Visweshwaran et al. 2024; Lü et al. 2011; Zha et al. 2019; Seo et al. 2021) or updating the underlying PTF constants (Pinnington et al. 2021; Cooper, Blyth, et al. 2021) to enhance predictive accuracy. Particularly, for JULES Pinnington et al. (2020) developed the Land Variational Ensemble Data Assimilation Framework (LAVENDAR), which was subsequently applied for parameter estimation to optimise the Toth PTF constants (Pinnington et al. 2021). Building on this Cooper, Blyth, et al. (2021) used the same framework to estimate Cosby PTF constants. Updating PTF constants is important, as it preserves the physical relationships between soil hydraulic parameters while reducing uncertainty propagation from poor calibration. When observations from multiple sites are assimilated jointly, they can yield a generalised set of posterior PTF constants. These capture diverse soil characteristics and can be applied to regions where in situ observations are unavailable.

Beyond parameters, the model's initial soil moisture condition also plays a significant role in model forecasts. While optimising model parameters minimises long-term bias (systematic error) in forecasts, state assimilation addresses stochastic errors (Nearing et al. 2018). The initial soil moisture condition influences not only current land surface processes but also future conditions through its long-term memory effect (Walker and Houser 2001). In practice, state estimation of soil moisture forms a key component of operational systems such as ERA5-Land and the ECMWF Integrated Forecasting System, where assimilation of moisture observations helps initialise land-surface conditions for short- to medium-range forecasts (Mahfouf and Viterbo 1996; Muñoz Sabater et al. 2021). Many studies have therefore focused on updating the initial soil moisture state

14698080, 2026, 5, Downloaded from https://rmets.onlinelibrary.wiley.com/doi/10.1002/met.70256 by UK Centre For Ecology & Hydrology, Wiley Online Library on [19/10/2026]. See the Terms and Conditions (https://onlinelibrary.wiley.com/terms-and-conditions) on Wiley Online Library for rules of use; OA articles are governed by the applicable Creative Commons License

in LSMs (Ridler et al. 2014; Dumedah and Walker 2014; Chen et al. 2015).

Accurate forecasting requires precise information on both the model parameters and initial conditions (Smith et al. 2013). While joint state-parameter estimation has been explored in other land surface models (Chen et al. 2015; Han et al. 2014), it remains unexplored in the context of the JULES model with ensemble-variational assimilation approaches. Although Pinnington et al. (2020) discussed the possibility of using LAVENDAR for state estimation, only parameter estimation was implemented. All subsequent applications with JULES (Pinnington et al. 2021; Cooper, Blyth, et al. 2021; Douglas et al. 2026) have been limited to parameter estimation only, without incorporating any state updates. Here, we introduce a novel extension by modifying the LAVENDAR algorithm to incorporate the state vector alongside the parameter vector in an augmented approach, enabling joint state-parameter estimation. This represents the first application of joint state-parameter assimilation for the JULES model, aiming to improve predictive accuracy across various soil characteristics. To demonstrate the advantage of state-parameter assimilation over individual state-only or parameter-only assimilation, in this study, we performed soil moisture assimilation in three scenarios:

1. parameter-only assimilation to update Cosby PTF constants (SC1),
2. state-only assimilation to update the initial soil moisture condition at the beginning of the assimilation period (SC2) (i.e., 1 January 2017) and
3. joint state-parameter assimilation to update both the initial soil moisture condition and Cosby PTF constants (SC3).

It should be noted that SC1 follows the same methodology as Cooper, Blyth, et al. (2021), using the same observation data (COSMOS-UK), assimilation period (2017), forecast period (2018) and PTF selection (Cosby). However, the experiments for SC1 were independently performed in this study and are not taken from Cooper, Blyth, et al. (2021) to ensure that exactly the same detailed JULES configuration was used in all of our experiments. SC1 is included here so that the comparison across all three scenarios can be followed within a single, self-contained study, without requiring reference to previous work. COSMOS-UK observations from 2017, across 16 sites in the UK, were integrated into the JULES model using an En-Var hybrid assimilation approach. Observations from all 16 sites were used together to derive common PTF constants representative of the different soil types in the UK and the model's initial conditions for each site.

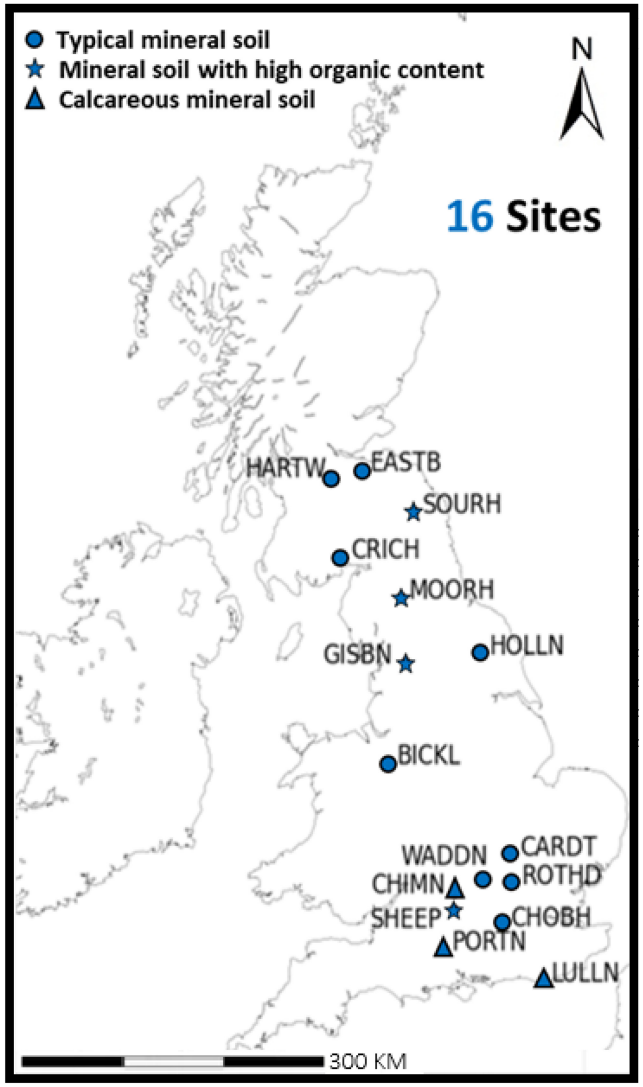


FIGURE 1 | Locations of the 16 COSMOS-UK sites used for assimilation, grouped by soil type. 'Typical mineral soil' sites: Cardington (CARDT), Bickley Hall (BICKL), Crichton (CRICH), Waddesdon (WADDN), Hollin Hill (HOLLN), Easter Bush (EASTB), Rothamsted (ROTHD), Hartwood Home (HARTW) and Chobham Common (CHOBH). 'High organic content' sites: Sheepdrove (SHEEP), Gisburn Forest (GISBN), Moorhouse (MOORH) and Sourhope (SOURH). 'Calcareous mineral soil' sites: Chimney Meadows (CHIMN), Porton Down (PORTN) and Lullington Heath (LULLN).

2 | Methods

2.1 | Study Area and COSMOS-UK Observations

To assess JULES performance during assimilation of field-scale soil moisture observations, 16 sites across the UK were selected (Figure 1). The sites were chosen based on the availability of COSMOS-UK soil moisture and meteorological observations over the assimilation and forecast period, while also seeking to ensure a representative range of soil types. The sites span three soil categories: typical mineral soil, high organic content and calcareous mineral soil. The details about the soil characteristics were taken from Antoniou et al. (n.d.).

The meteorological dataset required to run the JULES model was obtained from the COSMOS-UK sub-daily database (Cooper, Bennett, et al. 2021; Stanley et al. 2023). These data were collected every 30 min at the same 16 locations where soil moisture observations were measured. Meteorological observations from 2016 to 2018 were used in this study.

Soil moisture observations were obtained from the COSMOS-UK network. At each site, a Cosmic-Ray Neutron Sensor (CRNS)

14698080, 2026, 5, Downloaded from https://rmets.onlinelibrary.wiley.com/doi/10.1002/met.70256 by UK Centre For Ecology & Hydrology, Wiley Online Library on [19/10/2026]. See the Terms and Conditions (https://onlinelibrary.wiley.com/terms-and-conditions) on Wiley Online Library for rules of use; OA articles are governed by the applicable Creative Commons License

measures epithermal cosmic-ray neutrons attenuated by water molecules in the soil profile, providing near-real-time soil moisture integrated over a variable sensing depth that is reported alongside the dataset at a daily timestep (Evans et al. 2016). The sensor footprint covers an area of up to 120,000 m^2 and an effective depth of 10–80 cm, depending on local site conditions (Antoniou et al., n.d.). Observations are available at a 30-min temporal resolution and are calibrated at each site to account for local conditions (Evans et al. 2016). The integration of these observations into the assimilation system is detailed in Point 6 of Section 2.5.

2.2 | JULES Land Surface Model

JULES is a community land surface model that can operate independently or as the land surface component within the Met Office Unified Model (Best et al. 2011). Meteorological inputs required for running JULES include precipitation, wind speed, temperature, specific humidity, air pressure and incoming solar radiation. A detailed explanation of the energy and water flux components of JULES is provided in Best et al. (2011).

In this study, the focus is specifically on the soil hydraulic module of JULES, which governs the vertical redistribution of soil moisture within the soil profile. Other components of JULES such as canopy interception, surface runoff and throughfall govern the water input reaching the soil and remain active within the model structure in our experiments, but are not directly examined. Once water enters the soil surface, its vertical movement is calculated using a finite-difference form of Richards' equation, where the infiltrated water serves as the upper boundary condition and the free drainage defines the lower boundary. Although JULES can be configured with a variable number of soil layers, the default configuration of four vertical soil layers is used in this study to represent soil moisture, with thicknesses of 0.1, 0.25, 0.65 and 2 m. The water balance in each layer is expressed as

$$\frac{d\theta_l}{dt} = w'_{l-1} - w'_l - E'_l - R_{bl}, \tag{1}$$

where θ_l is the soil water content (in $m^3\ m^{-3}$) in layer l. The terms w'_{l-1} and w'_l represent the downward water flux infiltrating into layer l from the layer above $(l-1)$, and E'_l represents uptake by plant roots from soil layer l. All flux terms are expressed per unit layer thickness and have units of s^{-1}. the term R_{bl} denotes lateral flow, which is set to zero in this study, treating JULES as one-dimensional in vertical columns.

The vertical flux of water between soil layers (w'_l) is computed based on Darcy's law and depends on soil hydraulic properties. While JULES supports both the Brooks and Corey (n.d.) and van Genuchten (1980) formulations for soil hydraulic properties, the Brooks and Corey model is adopted here. The Brooks and Corey model is consistent with the PTFs that we use to derive the soil hydraulic parameters (see Section 2.3).

JULES represent the relationship between soil water content (θ in $m^3\ m^{-3}$), matric suction (ψ in m) and hydraulic conductivity (K_h in kg $m^{-2}\ s^{-1}$) as follows:

$$\frac{\theta}{\theta_{\text{sat}}} = \left(\frac{\psi}{\psi_{\text{sat}}}\right)^{-\frac{1}{b}}, \tag{2}$$

$$K_h = K_{h,\text{sat}}\left(\frac{\theta}{\theta_{\text{sat}}}\right)^{2b+3}, \tag{3}$$

where θ_{sat}, ψ_{sat} and $K_{h,\text{sat}}$ represent the volumetric soil moisture at saturation, matric suction at saturation and saturated hydraulic conductivity, respectively. The term b is the Clapp–Hornberger parameter that appears in the soil-water retention exponent.

2.3 | Pedotransfer Function

The soil hydraulic parameters (θ_{sat}, ψ_{sat} and $K_{\text{h,sat}}$) required by JULES (Equations 2 and 3) cannot be directly measured at the spatial scales relevant to LSMs. Direct measurements sample only small soil volumes and are expensive to deploy at the catchment or regional scales required by such models (Van Looy et al. 2017). PTFs are therefore employed to estimate these parameters from easily measurable properties like soil texture and specific density.

In this study, we adopt the Cosby PTF (Cosby et al. 1984; Marthews et al. 2014), a simple formulation which requires only soil sand and clay fractions as inputs, providing continuous functions well-suited for representing spatial heterogeneity across large scales. Further, the Cosby PTF has been used in conjunction with the JULES model across a wide range of UK soils and has shown promising results (Cooper, Blyth, et al. 2021).

The Cosby PTFs express each hydraulic parameter as a function of the clay and sand fractions by weight, f_{clay} and f_{sand}, through a set of empirical constants $C1$ to $C12$ whose prior values are given in table 2 of Cosby et al. (1984). The Clapp–Hornberger parameter (b), is defined as,

$$b = C1 + C2 f_{\text{clay}} - C3 f_{\text{sand}}. \tag{4}$$

The soil water content (θ_{sat}), which gives the maximum amount of water the soil can hold per unit volume when fully saturated is represented by,

$$\theta_{\text{sat}} = C4 - C5 f_{\text{clay}} - C6 f_{\text{sand}}. \tag{5}$$

The matric suction (ψ_{sat}), which describes the force with which water is held in the soil at saturation, is represented by,

$$\psi_{\text{sat}} = 0.01 \times 10^{(C7 - C8 f_{\text{clay}} - C9 f_{\text{sand}})}. \tag{6}$$

Finally, $K_{h,\text{sat}}$, which governs how easily water moves through the soil when fully saturated, is represented by,

$$K_{h,\text{sat}} = 10^{(-C10 - C11 f_{\text{clay}} + C12 f_{\text{sand}})}. \tag{7}$$

Other parameters are the critical point (θ_{crit}), wilting point (θ_{wilt}), dry soil heat capacity (h_{cap}) and thermal conductivity (h_{con}), are derived quantities that depend on θ_{sat} and ψ_{sat}. These represent, respectively, the water contents at which plant water

14698080, 2026, 5, Downloaded from https://rmets.onlinelibrary.wiley.com/doi/10.1002/met.70256 by UK Centre For Ecology & Hydrology, Wiley Online Library on [19/10/2026]. See the Terms and Conditions (https://onlinelibrary.wiley.com/terms-and-conditions) on Wiley Online Library for rules of use; OA articles are governed by the applicable Creative Commons License

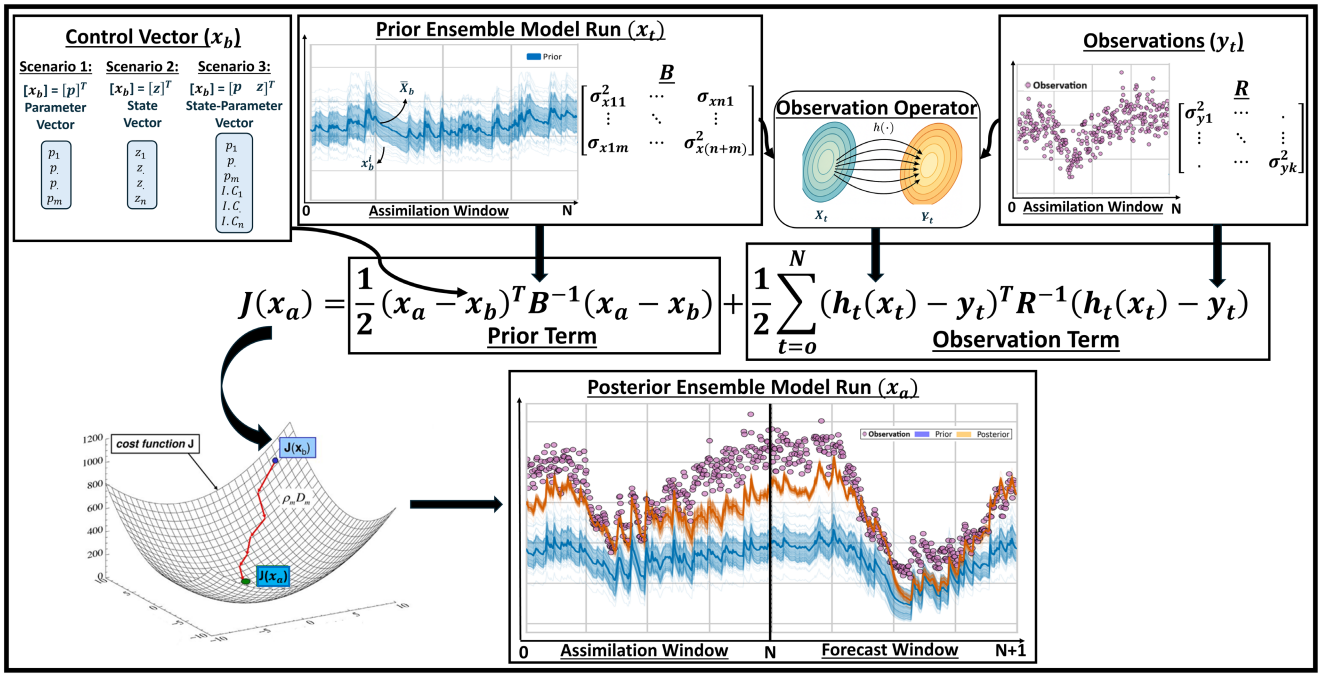


FIGURE 2 | Schematic diagram illustrating the components of the cost function (J).

uptake becomes limited and ceases, and the ability of the soil to store and transfer heat. Further details about the derived parameters can be found in Cooper, Blyth, et al. (2021) and Marthews et al. (2014).

2.4 | En-Var Assimilation

In this section, we describe how the JULES initial soil moisture condition and the PTF constants are updated using the En-Var assimilation approach. We consider the discrete non-linear dynamical model, written as

$$\mathbf{z}_t = \mathbf{f}_{t-1\to t}\left(\mathbf{z}_{t-1}, \mathbf{p}_{t-1}, \mathbf{z}_0\right), \tag{8}$$

where $\mathbf{z}_t \in \mathbb{R}^n$ represents the state vector at time t, and $\mathbf{p}_t \in \mathbb{R}^m$ denotes a vector of model parameters. The initial condition $\mathbf{z}_0$ provides the starting state for the model. The non-linear operator $\mathbf{f}$ propagates the state forward from $t-1$ to t ($t = 1, 2, \ldots, N$ timesteps). Here, JULES forms the model operator $\mathbf{f}$, which describes the evolution of soil moisture over time.

Model parameters are generally expected to be constant in time during a model forecast. However, in cycling data assimilation systems that include parameter estimation, parameters are typically updated after each assimilation window. For this reason, parameters are often expressed with a time index to indicate their dependence on the assimilation cycle. In this work, only a single assimilation window is used, spanning the year 2017. Nevertheless, the time-index notation is retained for flexibility in potential future applications involving multiple assimilation cycles.

Let $\mathbf{y}_t \in \mathbb{R}^{k_t}$ represent the observation vector at time t, which here comes from the COSMOS-UK soil moisture product. To enable a direct comparison with JULES soil moisture estimates, we use the observation operator $\mathbf{h}_t: \mathbb{R}^n \to \mathbb{R}^{k_t}$. The operator $\mathbf{h}_t$ maps the model state to the observation space and yields model-equivalent soil moisture estimates

$$\mathbf{y}_t = \mathbf{h}_t\left(\mathbf{z}_t\right) + \varepsilon_t, \tag{9}$$

where $\varepsilon_t \in \mathbb{R}^{k_t}$ is the observation error, assumed to be unbiased, Gaussian and uncorrelated in time, with a covariance matrix $\mathbf{R}_t$. These assumptions are standard in variational data assimilation and allow $\mathbf{R}_t$ to be specified as a diagonal matrix.

The En-Var method belongs to the class of variational assimilation techniques that uses a time window, drawing conceptual similarity to 4D-Var. Both approaches assimilate all observations from a predetermined time window and spatial domain together in a batch rather than sequentially. In the 4D-Var method, we seek to minimise the cost function $\mathbf{J}$, which includes two components:

i. The difference between the control vector $\mathbf{x}_t$ and its prior estimate ($\mathbf{x}_b$ representing the prior vector at time = 0, 'b' for 'background' synonymous with 'prior')
ii. The difference between modelled outputs and observations. Each component is weighted by the inverse of its respective error covariance matrix ($\mathbf{B}$ and $\mathbf{R}$). These matrices control the relative influence of observations and prior information in the final solution. The cost function ($\mathbf{J}$) is defined as

$$\mathbf{J}(\mathbf{x}_a) = \frac{1}{2}(\mathbf{x}_a - \mathbf{x}_b)^T \mathbf{B}^{-1}(\mathbf{x}_a - \mathbf{x}_b) + \frac{1}{2}\sum_{t=0}^{N}(\mathbf{h}_t(\mathbf{x}_t) - \mathbf{y}_t)^T \mathbf{R}^{-1}(\mathbf{h}_t(\mathbf{x}_t) - \mathbf{y}_t), \tag{10}$$

where N denotes the number of observation times used within the assimilation window. A simplified representation of different components of $\mathbf{J}$ is shown in Figure 2.

14698080, 2026, 5, Downloaded from https://rmets.onlinelibrary.wiley.com/doi/10.1002/met.70256 by UK Centre For Ecology & Hydrology, Wiley Online Library on [19/10/2026]. See the Terms and Conditions (https://onlinelibrary.wiley.com/terms-and-conditions) on Wiley Online Library for rules of use; OA articles are governed by the applicable Creative Commons License

The principal aim is to optimise a control vector $\mathbf{x}_t$ denoted by a set of variables that minimises $\mathbf{J}$. Generally, $\mathbf{x}_t$ is represented by a state ($\mathbf{z}$) and/or parameter vector ($\mathbf{p}$). In this study, the state vector represents a 1D soil column comprising four layers (Section 2.2), and the parameter vector is represented by the PTF constants (Section 2.3). Depending on the experiment, the control vector $\mathbf{x}_t$ may consist of $\mathbf{z}$, $\mathbf{p}$ or their concatenation $[\mathbf{p};\mathbf{z}]$. We do this in three ways (scenarios):

1. **Parameter-only assimilation (SC1)**: In this scenario, we evaluate the constants of the PTF (C1–C12; Equations 4–7), denoted by $\mathbf{p} \in \mathbb{R}^m$. Here, the control vector is represented as $\mathbf{x}_t = [\mathbf{p}_t]^T \in \mathbb{R}^m$, where $m = 12$ represents the 12 Cosby constants.
2. **State-only assimilation (SC2):** In this scenario, we estimate the initial soil moisture states $\mathbf{z}_0 \in \mathbb{R}^n$ consisting of the four soil layers at each of the 16 sites (Equation 1). The control vector for this scenario is represented as $\mathbf{x}_t = [\mathbf{z}_0]^T \in \mathbb{R}^n$, where $n = 64$.
3. **Joint state-parameter assimilation (SC3)**: In this scenario, we simultaneously estimate both the initial soil moisture states and the PTF constants. The augmented system control vector $\mathbf{x}_t$ is determined by appending the parameters to the model state vector. It is represented as $\mathbf{x}_t = [\mathbf{p}_t \ \ \mathbf{z}_0]^T \in \mathbb{R}^{m+n}$, where $m + n = 76$.

The state that minimises the cost function is often called the analysis or posterior vector ($\mathbf{x}_a$, 'a' for 'analysis' synonymous with 'posterior'). In practice, $\mathbf{x}_a$ is determined by iteratively minimising $\mathbf{J}$ using gradient-based optimisation (e.g., quasi-Newton or conjugate-gradient methods).

In En-Var, an ensemble is used to provide a flow-dependent estimate of the background error covariance matrix $\mathbf{B}$. To avoid calculating the tangent linear model, adjoint model and $\mathbf{B}^{-1}$ for JULES, En-Var applies a control variable transform to precondition the matrix $\mathbf{B}$ (Pinnington et al. 2020). This approach allows $\mathbf{B}$ to be defined as the product of the perturbation matrix, $\mathbf{X}'_b$, and its transpose, given by

$$\mathbf{B} \approx \mathbf{X}'_b \mathbf{X}'^{T}_b, \tag{11}$$

where

$$\mathbf{X}'_b = \frac{1}{\sqrt{N_e - 1}} \left(\mathbf{x}_b^{(1)} - \overline{\mathbf{x}_b}, \ \mathbf{x}_b^{(2)} - \overline{\mathbf{x}_b}, \ \ldots, \ \mathbf{x}_b^{(N_e)} - \overline{\mathbf{x}_b} \right). \tag{12}$$

The columns of $\mathbf{X}'_b$ are the deviations of each background ensemble member from the ensemble mean, $\overline{\mathbf{x}_b}$, where N_e is the ensemble size. The term $\mathbf{x}_b^{(i)}$ can come from a previous forecast (in that case $\overline{\mathbf{x}_b}$ is the mean of the N_e ensemble members) or sampled from a known distribution $\mathcal{N}(\overline{\mathbf{x}_b}, \mathbf{B})$. The posterior vector $\mathbf{x}_a$ is then defined as

$$\mathbf{x}_a = \overline{\mathbf{x}_b} + \mathbf{X}'_b \mathbf{w}, \tag{13}$$

where $\mathbf{w}$ is a weight vector of length N_e. Substituting Equations (13) and (11) into 10, we get a new cost function and its gradient as a function of $\mathbf{w}$ given by

$$\mathbf{J}(\mathbf{w}) = \frac{1}{2}\mathbf{w}^T\mathbf{w} + \frac{1}{2}\sum_{t=0}^{N} \left(\mathbf{Y}'_{b,t}\mathbf{w} + \mathbf{h}_t(\overline{\mathbf{x}_b}) - \mathbf{y}_t \right)^T \mathbf{R}^{-1} \left(\mathbf{Y}'_{b,t}\mathbf{w} + \mathbf{h}_t(\overline{\mathbf{x}_b}) - \mathbf{y}_t \right), \tag{14}$$

and

$$\nabla \mathbf{J}(\mathbf{w}) = \mathbf{w} + \sum_{t=0}^{N} \left(\mathbf{Y}'_{b,t} \right)^T \mathbf{R}^{-1} \left(\mathbf{Y}'_{b,t}\mathbf{w} + \widehat{\mathbf{h}}_t(\overline{\mathbf{x}_b}) - \widehat{\mathbf{y}}_t \right). \tag{15}$$

The term $\sum_{t=0}^{N} \mathbf{Y}'_{b,t} \approx \sum_{t=0}^{N} \mathbf{H}_t(\mathbf{X}'_b)$ is the perturbation matrix in observation space, and it is computed by

$$\mathbf{Y}'_{b,t} = \frac{1}{\sqrt{N_e - 1}} \left(\mathbf{h}_t\left(\mathbf{x}_b^{(1)}\right) - \mathbf{h}_t(\overline{\mathbf{x}_b}), \ \mathbf{h}_t\left(\mathbf{x}_b^{(2)}\right) - \mathbf{h}_t(\overline{\mathbf{x}_b}), \ \ldots, \ \mathbf{h}_t\left(\mathbf{x}_b^{(N_e-1)}\right) - \mathbf{h}_t(\overline{\mathbf{x}_b}), \ \mathbf{h}_t\left(\mathbf{x}_b^{(N_e)}\right) - \mathbf{h}_t(\overline{\mathbf{x}_b}) \right). \tag{16}$$

This allows the computation of the posterior without explicitly determining the tangent linear model, adjoint model and $\mathbf{B}^{-1}$. Minimising the cost function (Equation 14) using the gradient provides the posterior estimate of $\mathbf{w}$, which, when substituted into Equation (13), yields the posterior estimate of the control vector $\mathbf{x}_a$. The posterior ensemble perturbations, representing the uncertainty in the analysis, are obtained from the Hessian of the cost function following (Douglas et al. 2025) as

$$\mathbf{X}'_a \approx \mathbf{X}'_b \left(\mathbf{I} + \sum_{t=0}^{N_e} \left(\mathbf{Y}'_{b,t} \right)^T \mathbf{R}^{-1} \mathbf{Y}'_{b,t} \right)^{-\frac{1}{2}}. \tag{17}$$

2.5 | Experiment Design

The experiment was performed for 3 years between 2016 and 2018. The year 2016 was designated as the spin-up period to initialise the JULES model, 2017 served as the assimilation window for the En-Var implementation, and 2018 was used for forecast evaluation of JULES after assimilation. The implementation of COSMOS-UK soil moisture assimilation into the JULES model using the En-Var is done in three scenarios as outlined in Section 2.4. The key elements involved in the implementation of these three scenarios are outlined below and shown in Figure 3.

1. **Ensemble generation**: A 50-member ensemble (i.e., $N_e = 50$) was generated for each of the 12 Cosby PTF constants by sampling from a Gaussian distribution centred on the mean values reported by Cosby et al. (1984), with a standard deviation equal to 10% of the mean. The ensemble size of 50 is consistent with previous applications of the LAVENDAR framework (Cooper, Blyth, et al. 2021; Pinnington et al. 2020). This ±10% standard deviation range was chosen as a practical estimate to introduce variability around the prior values, informed by previous and successful experience with JULES on these sites by Cooper, Blyth, et al. (2021).
2. **Harmonised World Soil Database (HWSD)**: Soil texture information, comprising the percentage of sand, silt and clay, is obtained from the HWSD dataset (Fischer et al., n.d.) for all 16 sites. The HWSD data, originally in a 30 arc-second spatial scale gridded raster format, were

14698080, 2026, 5, Downloaded from https://rmets.onlinelibrary.wiley.com/doi/10.1002/met.70256 by UK Centre For Ecology & Hydrology, Wiley Online Library on [19/10/2026]. See the Terms and Conditions (https://onlinelibrary.wiley.com/terms-and-conditions) on Wiley Online Library for rules of use; OA articles are governed by the applicable Creative Commons License

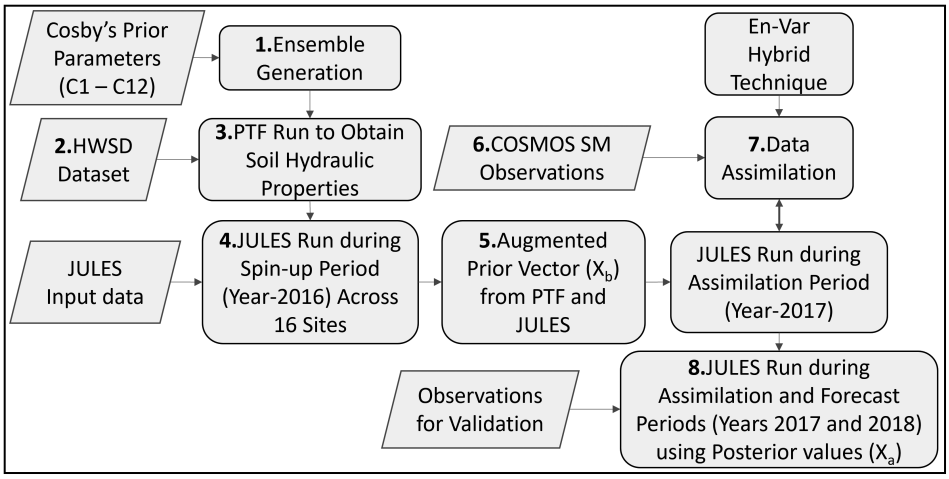


FIGURE 3 | Schematic showing the application of the En-Var assimilation scheme on the JULES land surface model during state-parameter estimation (SC3). The numbered components represent the key elements of the proposed methodology adopted in this study. Detailed explanations of each element are provided in Section 2.5.

downscaled to a 1 km resolution, and the gridpoints passing through the COSMOS-UK sites were selected. It should be noted that the HWSD soil texture data were selected to ensure consistency across sites and to adopt realistic UK-scale applications where local measurements are often unavailable. While discrepancies with site-specific data exist, HWSD has been successfully used in previous JULES studies (Martínez-de la Torre et al. 2019; Ritchie et al. 2019). Building on this prior success and given its relevance to large-scale applications, HWSD was chosen for this study.

3. **Pedotransfer function**: Cosby PTF is applied using the HWSD data, and the $_{C1-C12}$ sets are used to generate a 50-member ensemble of unique soil hydraulic parameters. It should be noted that a prior sensitivity analysis to select a subset of parameters is not required, since all 12 PTF constants are included in the estimation.

4. **Spin-up period**: The soil hydraulic parameters (50×12) obtained from the PTF are fed into the JULES model during the warm-up period extending from January to December 2016.

5. **Prior vector**:
   a. **Scenario 1 (SC1)**: During parameter estimation, Cosby's prior parameter 50-member ensemble, which is common to all 16 sites, forms the prior ensemble with a dimension of $\left\{\mathbf{x}_b^{(i)} \in \mathbb{R}^{12} : i = 1, 2, \ldots, 50\right\}$.
   b. **Scenario 2 (SC2)**: During state estimation, the JULES 50-member ensemble forecast at the end of the spin-up period, represented by four soil layers, forms the initial soil moisture condition for the start of the assimilation period. These 4 layers for each of the 16 sites are combined to represent the prior ensemble (i.e., $\left\{\mathbf{x}_b^{(i)} \in \mathbb{R}^{64} : i = 1, 2, \ldots, 50\right\}$).
   c. **Scenario 3 (SC3)**: During state-parameter estimation, JULES 50-member ensemble forecast (containing 4 soil layers) from the spin-up period for each site and a common Cosby's prior parameter ensemble representing all the 16 sites are augmented to represent the prior ensemble (i.e., $\left\{\mathbf{x}_b^{(i)} \in \mathbb{R}^{76} : i = 1, 2, \ldots, 50\right\}$).

6. **Observations**:
   a. **Observation Operator**: As outlined in Section 2.1, COSMOS-UK provides soil moisture observations at the field scale around the CRNS instrument at a 30-min frequency. We require the JULES soil moisture values to correspond to the same soil depth as the observations. Therefore, a weighted depth approach is employed, averaging the JULES estimates over the top soil layers to align with the effective sensing depth of COSMOS-UK. The sensing depth varies with soil moisture, but typically does not extend to the bottom layer of JULES (Antoniou et al., n.d.; Evans et al. 2016), which is therefore excluded from the weighted average. Assimilation updates, however, still influence deeper layers due to strong vertical correlations in the background error covariance matrix. Further details on the weighted depth approach can be found in Cooper, Blyth, et al. (2021).
   b. **Observation Uncertainties**: Half-hourly observations are averaged to a daily scale for our experiments. Analysis indicates that the standard deviation of half-hourly data around the daily mean is approximately 20% (Cooper, Blyth, et al. 2021). However, in the data assimilation framework, the observation error must also account for errors in the conversion of neutron counts to soil moisture, the averaging of sub-daily measurements to a daily scale and temporal (intra-site) observation error correlations arising from persistent calibration or environmental effects at a given site. We also recognise the presence of representation errors (Janjić et al. 2018), which may result from differences in scale between the model and the observations, or simplifications in the observation operator. To account for these additional sources of uncertainty, we inflate the standard deviation to 50% of the daily mean observation when assigning $\mathbf{R}$, consistent with practices adopted in

14698080, 2026, 5, Downloaded from https://rmets.onlinelibrary.wiley.com/doi/10.1002/met.70256 by UK Centre For Ecology & Hydrology, Wiley Online Library on [19/10/2026]. See the Terms and Conditions (https://onlinelibrary.wiley.com/terms-and-conditions) on Wiley Online Library for rules of use; OA articles are governed by the applicable Creative Commons License

other data assimilation studies (Liu and Rabier 2003; Stewart et al. 2008).

7. **Data assimilation**: The En-Var assimilation scheme is employed within the JULES model for the year 2017, using a one-year time window to ensure that the hydraulic parameters are constrained against a full seasonal cycle of soil moisture variability. This produces posterior values for the state (for each site) and/or parameters (common for all sites).
8. **Model forecast**: 3 and 4 are repeated with posterior PTF values, and the JULES model is rerun for the assimilation period (year 2017) and for the forecast period (year 2018) with the posterior initial conditions and soil ancillary files.

2.6 | Evaluation Metrics

To assess the model's performance during assimilation and forecast periods, two evaluation metrics are calculated: Root Mean Square Error (RMSE) and Kling-Gupta Efficiency (KGE). These metrics enable a comprehensive assessment of the model's performance by quantifying discrepancies between observed and modelled soil moisture values over a two-year period. The RMSE and KGE metrics are defined as follows:

$$\mathrm{RMSE} = \sqrt{\frac{\sum_{t=1}^{N} \left(\theta_m^t - \theta_o^t\right)^2}{N}}, \tag{18}$$

where N is the total number of observations. In this study, $N = 730$ for the two-year study period, and θ_m and θ_o are the modelled and observed soil moisture values, respectively. The term KGE is defined as

$$\mathrm{KGE} = 1 - \sqrt{(r-1)^2 + (\alpha-1)^2 + (\beta-1)^2}. \tag{19}$$

The KGE, as proposed by Gupta et al. (2009), provides an overall assessment of soil moisture distribution trends by incorporating three components: correlation, variability and bias. In this context, r represents the Pearson correlation coefficient, capturing the correlation between modelled and observed soil moisture time series. The term $\alpha = \sigma_m / \sigma_o$ reflects the model's ability to capture the variability in the observations, where σ_m and σ_o are the standard deviations of the modelled and observed data, respectively. Meanwhile, $\beta = \mu_m / \mu_o$ represents the model bias, where μ_m and μ_o denote the mean soil moisture values for the model and observations. Together, these components provide a robust evaluation of model performance. For all components and the KGE, values closer to 1 indicate good model performance.

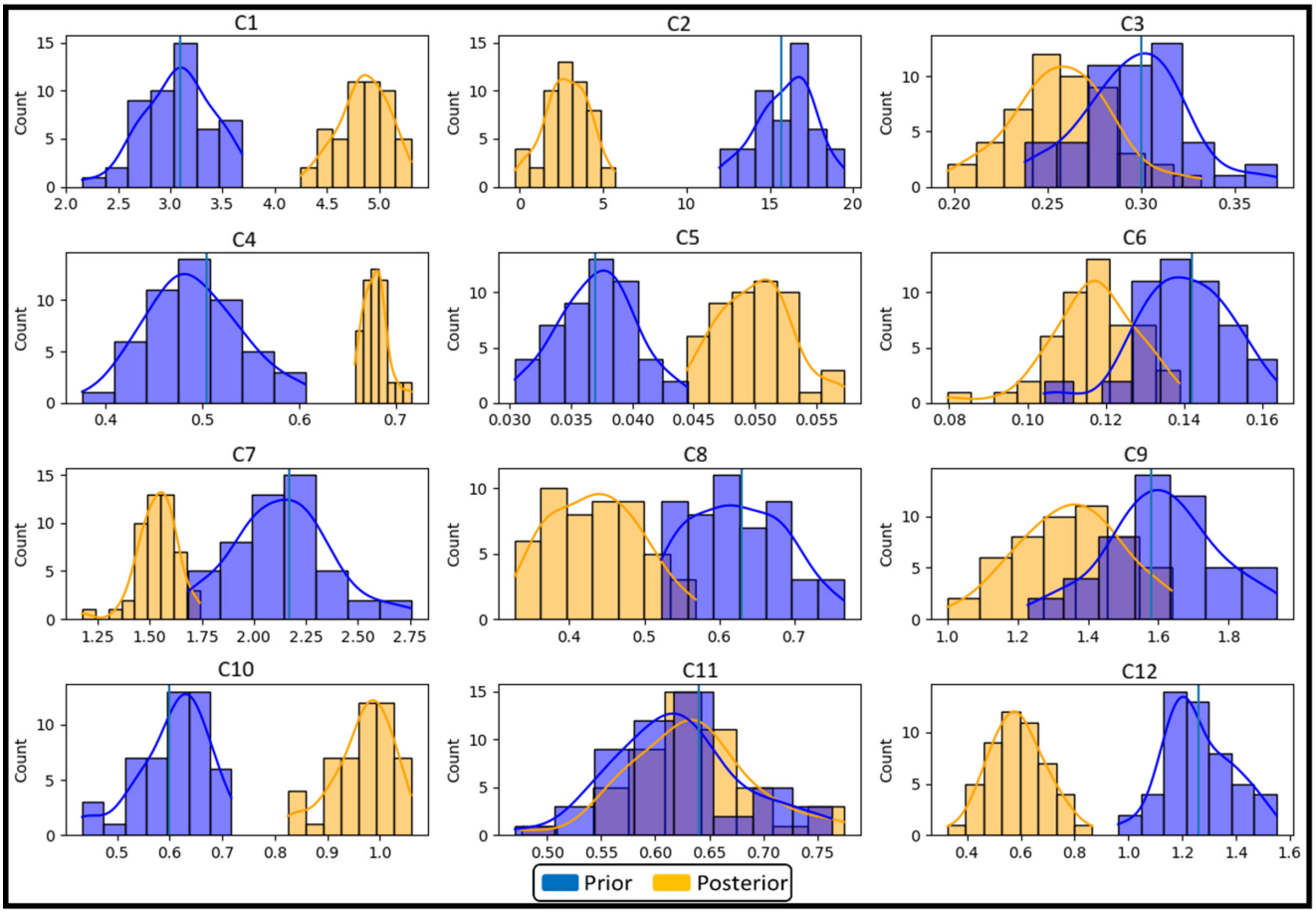


FIGURE 4 | Histograms showing the prior and posterior distribution values of Cosby PTF constants ($C1$ to $C12$) during parameter-only assimilation scenario (SC1) across 16 sites. Blue (prior) and orange (posterior) lines represent kernel density estimates. Bin widths are individually adjusted to reflect the range and spread of values for each constant.

14698080, 2026, 5, Downloaded from https://rmets.onlinelibrary.wiley.com/doi/10.1002/met.70256 by UK Centre For Ecology & Hydrology, Wiley Online Library on [19/10/2026]. See the Terms and Conditions (https://onlinelibrary.wiley.com/terms-and-conditions) on Wiley Online Library for rules of use; OA articles are governed by the applicable Creative Commons License

3 | Results

3.1 | Scenario 1: Individual Effect of Parameter Assimilation on JULES Performance

During parameter-only assimilation (SC1), Cosby PTF constants were updated and this scenario is included as a baseline following (Cooper, Blyth, et al. 2021) to enable direct comparison with SC2 and SC3. The resulting changes in the PTF constants led to corresponding shifts in the derived hydraulic parameters, as shown in Figures 4 and 5. For instance, the parameter θ_{sat} increased due to higher values of $C4$ and $C5$, suggesting an increase in the model's representation of the soil's water-holding capacity at full saturation. In contrast, $K_{h,sat}$ decreased due to changes in $C10$ to $C12$ values. This indicates that the model now simulates slower water movement through the soil when fully saturated, which may suggest less permeable soil conditions in the model. In addition, parameters ψ_{sat} and b were reduced due to the decreased values of $C7$ to $C9$ and changes in $C1$ to $C3$ values, respectively. Finally, θ_{crit} and θ_{wilt} showed only small differences between prior and posterior distributions, but they remain relevant as indicators of shifts in plant-available water and soil moisture retention characteristics following data assimilation. Overall, the posterior distributions are narrower than the prior distributions across all sites, since the En-Var technique serves as an approximate minimum variance estimator.

Figure 6 shows the ensemble mean JULES and COSMOS-UK soil moisture time series for the HOLLN and SHEEP sites, which have different soil characteristics. It is evident that the posterior soil moisture time series is more consistent with the COSMOS-UK observations than the prior values. Both KGE (Figure 7) and RMSE (Table 1) metrics also showed a similar outcome. Although Figure 4 and Table 1 include results from the other scenarios, this section discusses SC1 specifically. The posterior RMSE values decreased relative to the prior values, with an average reduction of 49% across all 16 sites. For the KGE metrics, improvements were mainly driven by reductions in the α and β components (capturing variability and bias). This is due to changes in θ_{sat}, b and $K_{h,sat}$, which increased soil water storage and reduced the underestimation in the JULES soil moisture estimates.

3.2 | Scenario 2: Individual Effect of State Assimilation on JULES Performance

During state assimilation, the initial soil moisture conditions at the start of the assimilation window (i.e., 1 January 2017) are updated for each site, and the posterior JULES estimates

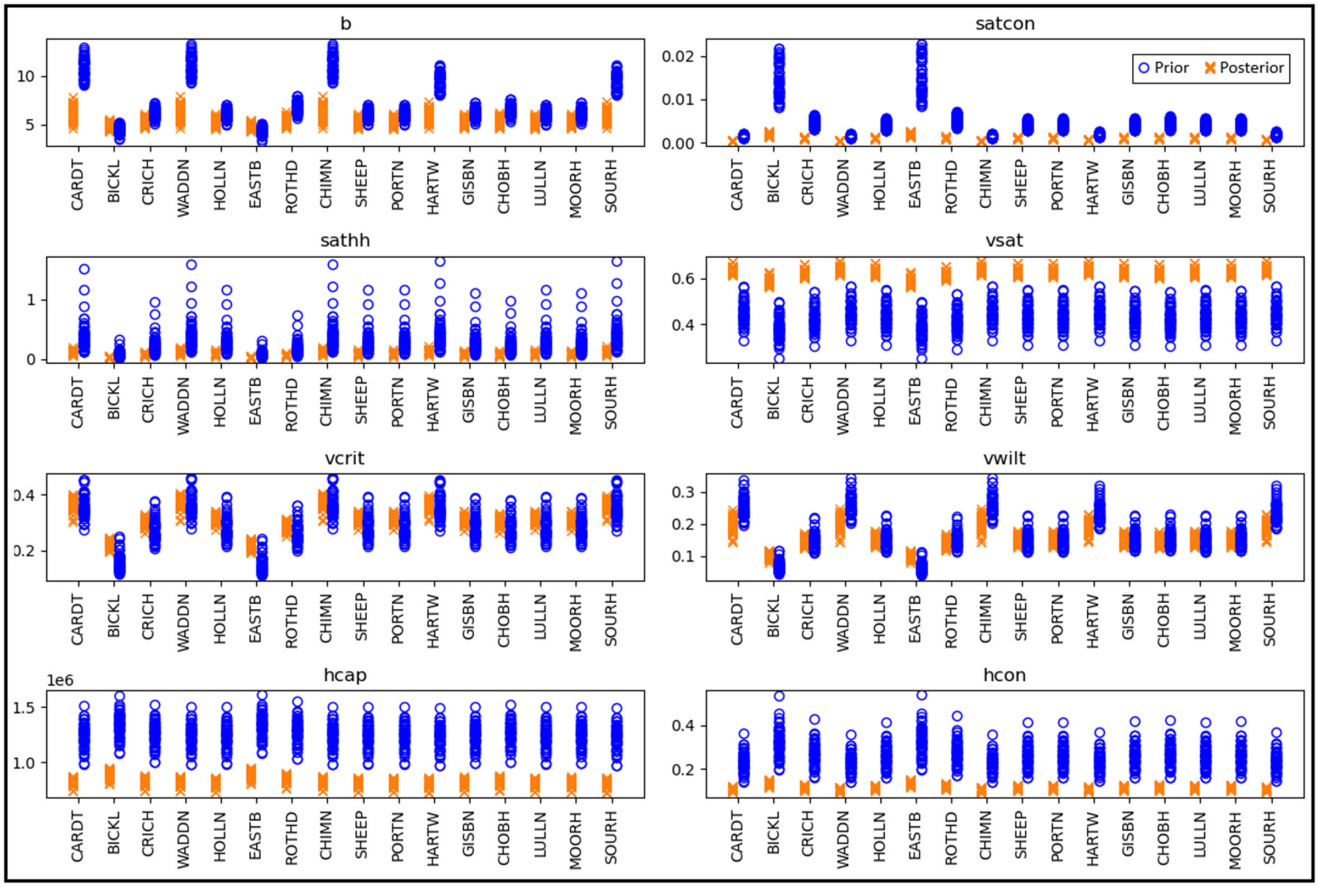


FIGURE 5 | Ensemble prior and posterior values of different soil hydraulic parameters at 16 sites across the UK during parameter-only assimilation scenario (SC1).

14698080, 2026, 5, Downloaded from https://rmets.onlinelibrary.wiley.com/doi/10.1002/met.70256 by UK Centre For Ecology & Hydrology, Wiley Online Library on [19/10/2026]. See the Terms and Conditions (https://onlinelibrary.wiley.com/terms-and-conditions) on Wiley Online Library for rules of use; OA articles are governed by the applicable Creative Commons License

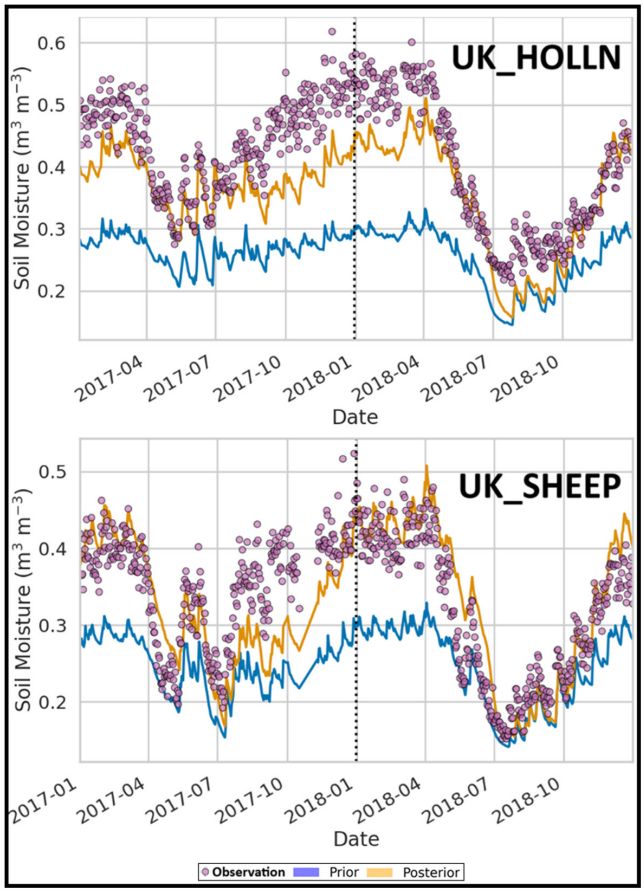


FIGURE 6 | Modelled (ensemble mean) and observed soil moisture time series at HOLLN and SHEEP sites during assimilation (2017) and forecast periods (2018) for parameter-only assimilation scenario (SC1).

TABLE 1 | RMSE values between the JULES simulated soil moisture and COSMOS-UK observations during different scenarios.

	RMSE (m^3 m^{-3})			
Site	Prior	Posterior parameter-only (SC1)	Posterior state-only (SC2)	Posterior state-parameter (SC3)
CARDT	0.09	0.08	0.07	0.08
BICKL	0.14	0.03	0.08	0.03
CRICH	0.12	0.04	0.06	0.04
WADDN	0.10	0.07	0.06	0.07
HOLLN	0.17	0.06	0.10	0.06
EASTB	0.16	0.04	0.10	0.03
ROTHD	0.08	0.04	0.03	0.04
CHIMN	0.06	0.05	0.06	0.05
SHEEP	0.10	0.05	0.05	0.05
PORTN	0.11	0.07	0.06	0.06
HARTW	0.17	0.10	0.10	0.10
GISBN	0.23	0.09	0.17	0.07
CHOBH	0.28	0.20	0.21	0.20
LULLN	0.09	0.04	0.04	0.04
MOORH	0.25	0.13	0.17	0.11
SOURH	0.13	0.07	0.08	0.06
Average	0.143	0.073	0.09	0.068

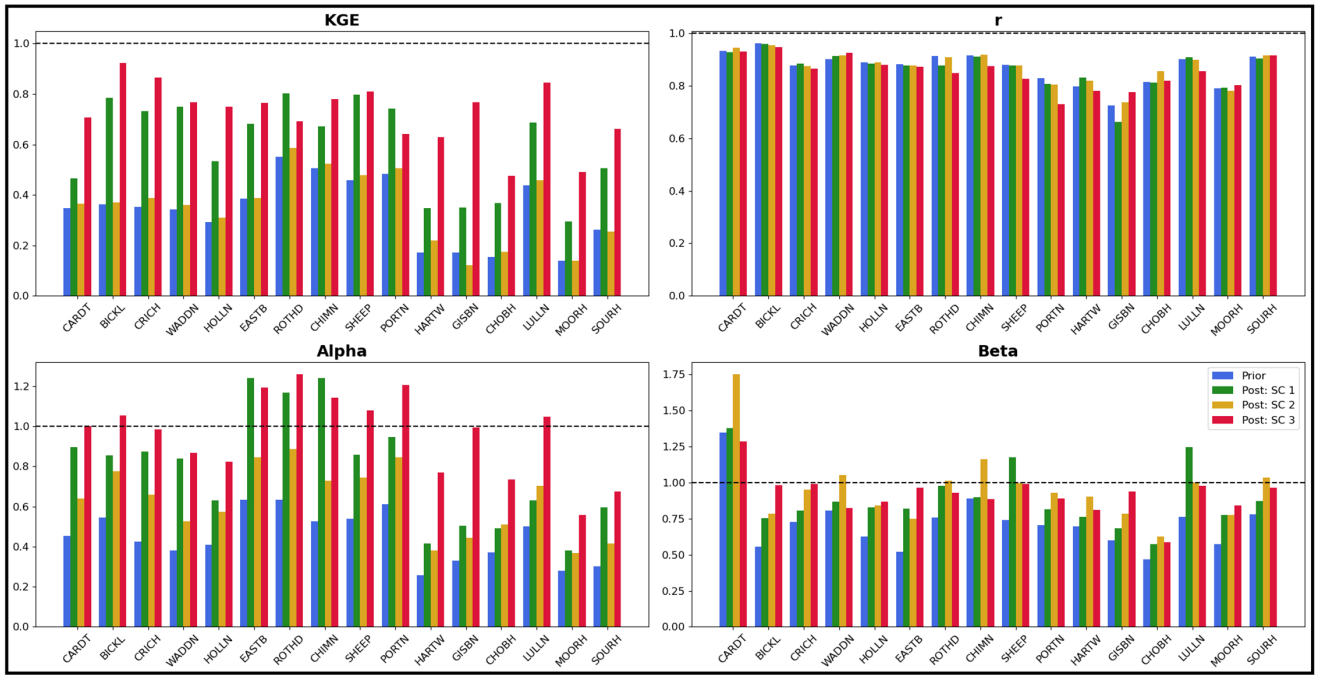


FIGURE 7 | KGE metrics and its components showing the performance of JULES model across all the 16 sites in the UK for three assimilation scenarios: Parameter-only (SC1), state-only (SC2) and joint state-parameter (SC3).

14698080, 2026, 5, Downloaded from https://rmets.onlinelibrary.wiley.com/doi/10.1002/met.70256 by UK Centre For Ecology & Hydrology, Wiley Online Library on [19/10/2026]. See the Terms and Conditions (https://onlinelibrary.wiley.com/terms-and-conditions) on Wiley Online Library for rules of use; OA articles are governed by the applicable Creative Commons License

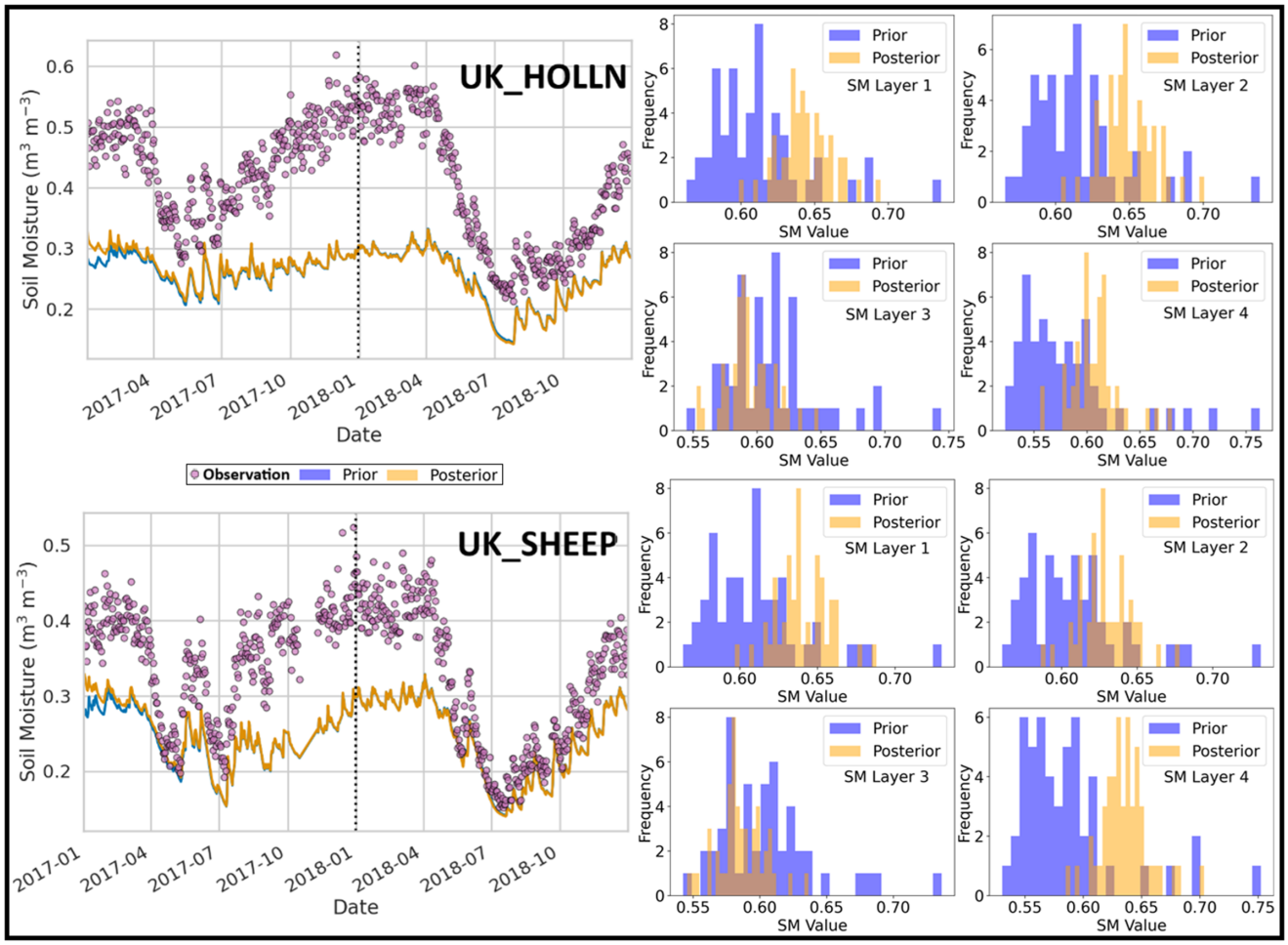


FIGURE 8 | The figure shows the results of the state-only assimilation scenario (SC2). The left panels display the modelled (ensemble mean) and observed soil moisture time series at the HOLLN and SHEEP sites during the assimilation (2017) and forecast (2018) periods. The right panels show the prior and posterior distributions of the initial condition state (1 January 2017) across 50 ensemble members and four soil layers.

($\mathbf{x}_a$) are compared against COSMOS-UK observations. The adjustments made to the initial conditions shifted the posterior estimates closer to the observations during the initial phase (January 2017–April 2017), as illustrated in Figure 8 with examples from the HOLLN and SHEEP sites. These sites were chosen to represent two distinct soil types—typical mineral soil (HOLLN) and soil with high organic content (SHEEP)—since JULES performance is likely to vary depending on soil characteristics. Although assimilating the initial conditions improved the JULES estimates, the improvement progressively weakened after approximately 4–5 months. Notably, for most sites, including HOLLN and SHEEP, both the prior and posterior estimates showed no significant differences after 6 months. This reflects the limited memory and dynamic response of soil moisture to ongoing meteorological forcing over longer durations (seasonal to annual timescales).

While analysing the RMSE (Table 1) and KGE (Figure 7) metrics, we observe moderate improvements relative to the prior run. The RMSE values decreased across all sites, with an average reduction of 37.1 % over the 16 sites. Correspondingly, KGE values showed a moderate improvement between the prior (blue) and posterior (brown) estimates for most sites, except at GISBN. The anomaly at GISBN may be related to the dense coniferous cover, which affects CRNS calibration and reduces the reliability of COSMOS-UK soil moisture retrievals. Component-wise, improvements were mainly reflected in the α and β terms, while the correlation component r changed little due to the already high correlation between the prior model estimates and observations before assimilation. Although these improvements were observed, the parameter-only scenario (SC1) clearly outperformed the state-only scenario (SC2), which can be attributed to the rapid decay of the impact of the updated initial soil moisture state.

3.3 | Scenario 3: Combined Effect of State-Parameter Assimilation on JULES Performance

During joint state-parameter assimilation, we optimised both Cosby constants and JULES's initial soil moisture condition. Figure 9 shows that the posterior parameter distribution (orange) deviated from its respective prior distribution (blue) after assimilation, though the deviations are less pronounced compared to the parameter-only scenario. This suggests that updating the initial soil moisture conditions in this scenario has partially alleviated the adjustments required in the PTF constants. Due to this, all eight soil hydraulic properties in

14698080, 2026, 5, Downloaded from https://rmets.onlinelibrary.wiley.com/doi/10.1002/met.70256 by UK Centre For Ecology & Hydrology, Wiley Online Library on [19/10/2026]. See the Terms and Conditions (https://onlinelibrary.wiley.com/terms-and-conditions) on Wiley Online Library for rules of use; OA articles are governed by the applicable Creative Commons License

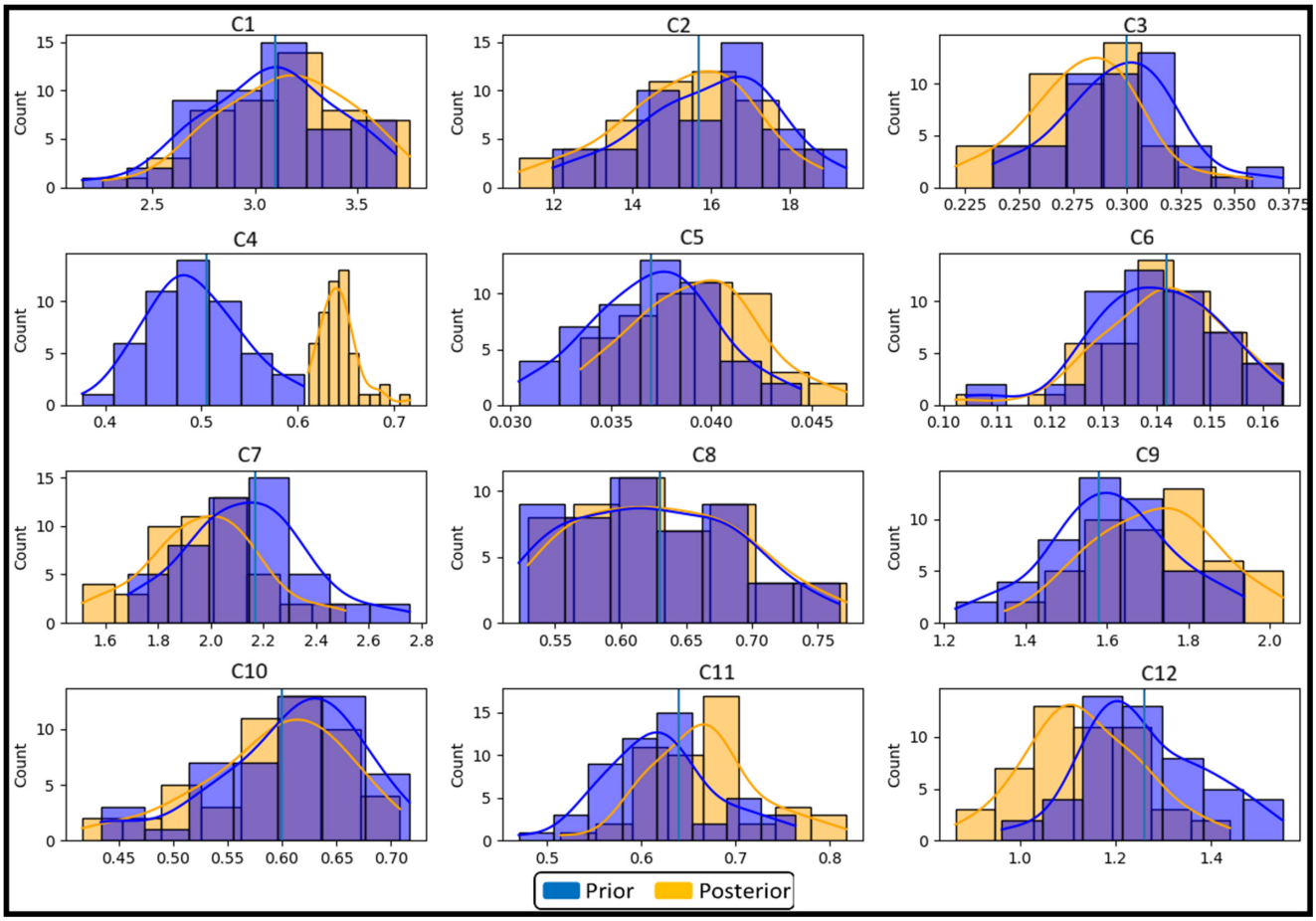


FIGURE 9 | Histograms showing the prior and posterior distribution values of Cosby PTF constants ($C1$ to $C12$) during state-parameter assimilation (SC3) across 16 sites. Blue (prior) and orange (posterior) lines represent kernel density estimates. Bin widths are individually adjusted to reflect the range and spread of values for each constant.

the Brooks and Corey model also showed deviations from their respective prior values as shown in Figure 10. In general, across all sites, the ensemble members span a narrower range in the posterior distribution than in the prior distribution, as seen in the parameter-only assimilation scenario, suggesting a reduction in variability of the hydraulic parameters after assimilation.

After assimilation, the posterior JULES is able to store more water in the soil, due to the combined effect of increased retention capacity and reduced hydraulic conductivity. This is due to the changes observed in $K_{h,\mathrm{sat}}$ and θ_{sat} values. Parameter $K_{h,\mathrm{sat}}$ reduced due to the decreased $C10$ and $C12$ values, while the increase in θ_{sat} is driven by higher $C4$ and $C5$ values. It should be noted that the magnitude change in both θ_{sat} and $K_{\mathrm{h,sat}}$ is smaller than that observed in SC1. Finally, b and ψ_{sat} show only minimal shifts in their distributions after assimilation.

Similarly, Figure 11 shows the prior and posterior distribution of initial soil moisture conditions for two locations, GISBN and CARDT. These sites were selected to illustrate the assimilation's impact on different soil types—GISBN with high organic content and CARDT with mineral-rich soil. From the figure, we can see that the initial soil moisture condition has increased in GISBN and decreased in CARDT after assimilation. This is because, on January 1, 2017, the model's prior estimates were lower compared to the observations for the GISBN location and higher for the CARDT location. Accordingly, the initial condition was updated to be closer to the observation values. The prior and posterior distributions for all 16 locations are shown in Figures A1–A4 of Appendix A.

Figure 12 shows the ensemble mean soil moisture time series for two locations with different soil characteristics. Table 1 and Figure 12 show that the posterior soil moisture estimates are more consistent with the COSMOS-UK observations than the prior estimates. RMSE reduced by an average of 50% across all sites, with the maximum reduction observed at BICKL (78.5%) followed by GISBN (69.5%). Overall, these results suggest that the bias in the model is significantly reduced, the posterior JULES estimates showed a good correlation with COSMOS-UK observations, and the variability in the observations is captured more accurately.

KGE values showed significant improvement after assimilation, with the maximum increase observed at the GISBN site ($\approx$ 350%) and a minimum increase of $\approx$ 25% at the CHIMN site

14698080, 2026, 5, Downloaded from https://rmets.onlinelibrary.wiley.com/doi/10.1002/met.70256 by UK Centre For Ecology & Hydrology, Wiley Online Library on [19/10/2026]. See the Terms and Conditions (https://onlinelibrary.wiley.com/terms-and-conditions) on Wiley Online Library for rules of use; OA articles are governed by the applicable Creative Commons License

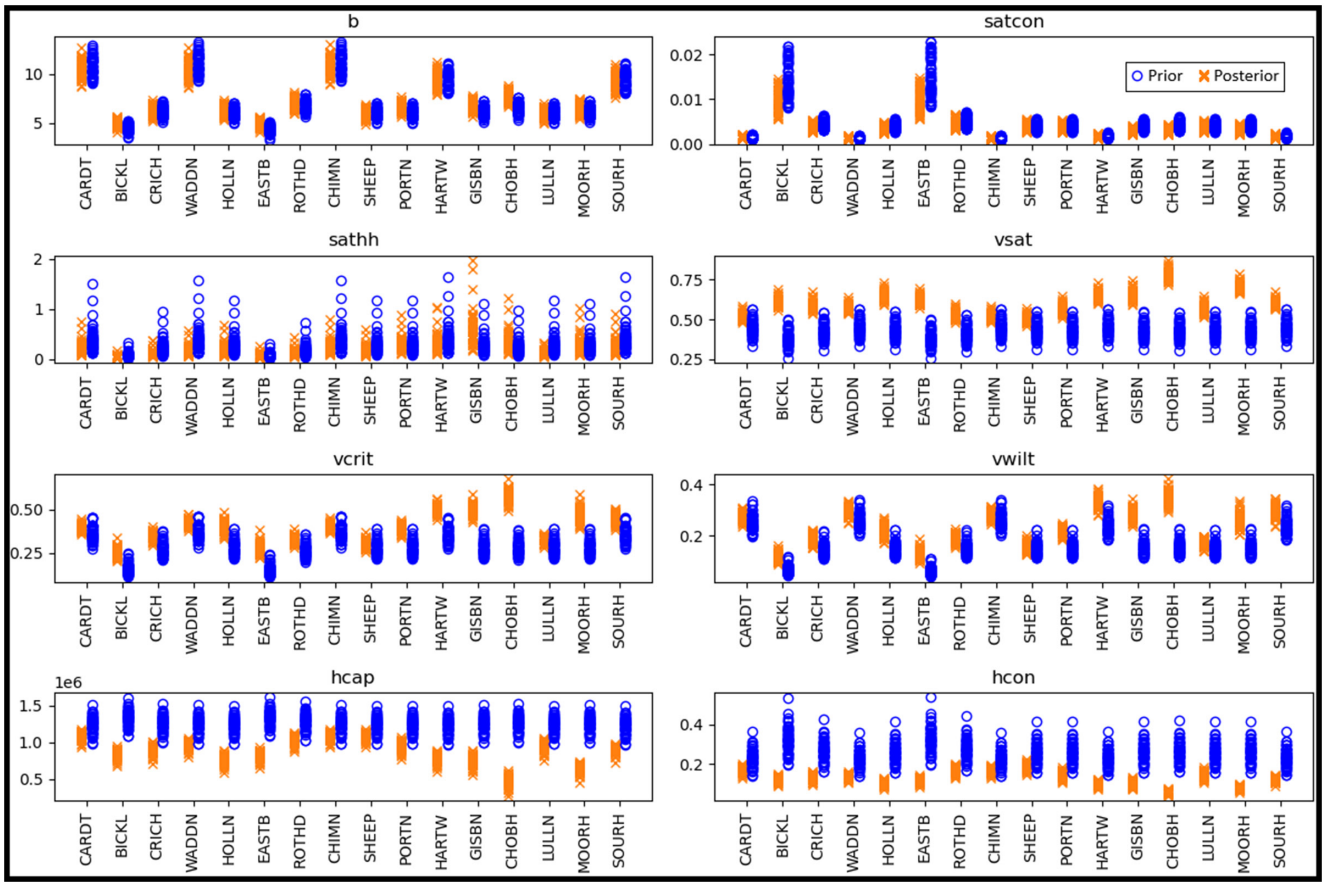


FIGURE 10 | Ensemble prior and posterior values of different soil hydraulic parameters at 16 sites across the UK during state-parameter assimilation scenario (SC3).

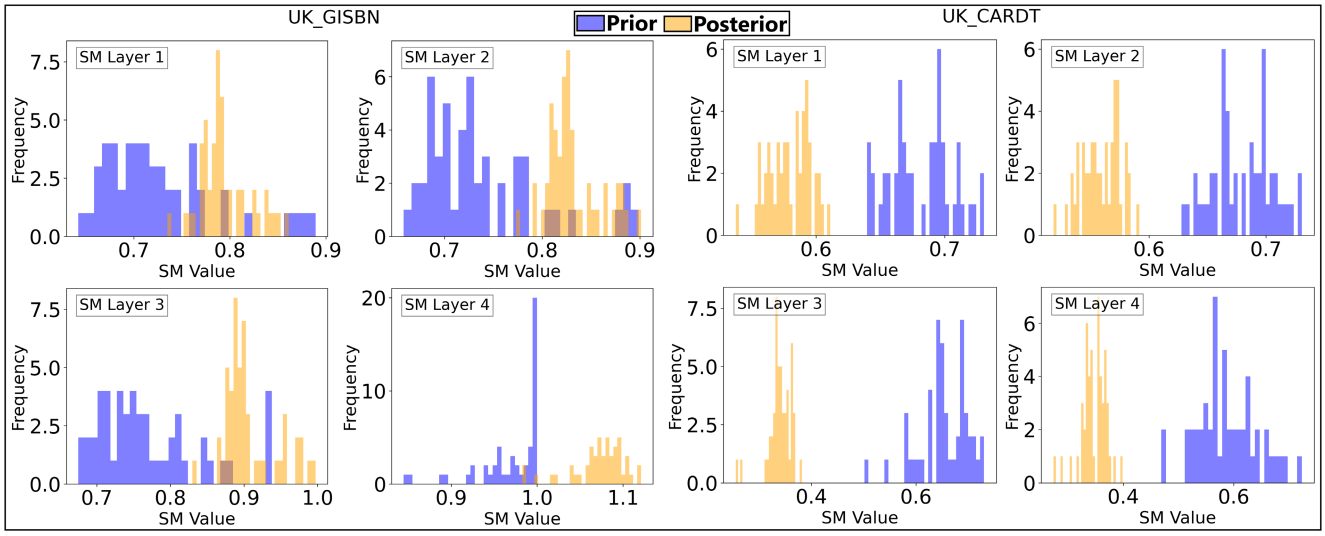


FIGURE 11 | Prior (blue) and posterior (orange) distributions of JULES's initial soil moisture condition during state-parameter assimilation (SC3) for two sites (GISBN and CARDT) across 50 ensemble members and four soil layers. Bin widths vary across subplots to allow comparison of prior and posterior value ranges for each soil layer.

(Figure 7). Breaking down the components of KGE, the combined effect of the α and β components contributed substantially to the increase in KGE. The r component was already high in the prior JULES estimates (averaging more than ≈ 0.8), leaving little scope for assimilation to improve the correlation with COSMOS-UK observations.

Out of the 16 locations, prior soil moisture estimates at 15 sites were negatively biased, as indicated by the β component (values less than 1, represented by a horizontal line). After assimilation, the hydraulic parameter $K_{h,\mathrm{sat}}$ decreased, reducing the movement of water within the soil profile, while the parameter θ_{sat} increased, improving the water holding capacity of the soil. This

14698080, 2026, 5, Downloaded from https://rmets.onlinelibrary.wiley.com/doi/10.1002/met.70256 by UK Centre For Ecology & Hydrology, Wiley Online Library on [19/10/2026]. See the Terms and Conditions (https://onlinelibrary.wiley.com/terms-and-conditions) on Wiley Online Library for rules of use; OA articles are governed by the applicable Creative Commons License

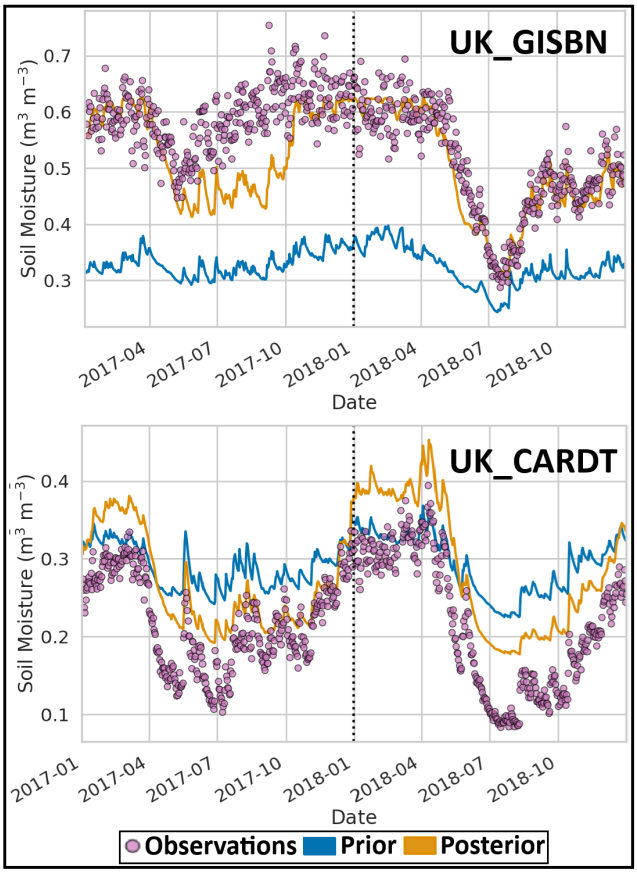


FIGURE 12 | Modelled (ensemble mean) and observed soil moisture at GISBN and CARDT sites during assimilation (2017) and forecast periods (2018) for state-parameter assimilation scenario (SC3).

combined effect increased the water content in the soil column, reducing the underestimation of the prior JULES run. This improvement also enabled the model to better capture the variability in COSMOS-UK observations, leading to an improved α component.

On average across the 16 sites, SC3 improved KGE by 113% relative to the prior, 9.6% relative to SC1 and 105% relative to SC2. A similar pattern is observed for the RMSE values. SC3 reduced RMSE by 52.4% relative to the prior, by 6.8% compared to SC1 and by 24.4% compared to SC2. Together, these results demonstrate that jointly updating both model states and PTF constants provides a more consistent improvement in soil moisture simulations than updating either component in isolation.

4 | Discussion

In general, results from all three scenarios demonstrated that assimilating field-scale soil moisture observations can improve the JULES performance. Comparing SC3 with SC1 and SC2 showed that joint state-parameter assimilation can constrain the JULES model well and enhance its predictive skill. Specifically, in SC3, the average KGE value increased from 0.33 to 0.72 after assimilation, corresponding to an improvement of approximately 113% relative to the prior. In contrast, individual state-only and parameter-only assimilation results showed moderate improvements of about 6% (KGE: 0.33–0.35) and 100% (KGE: 0.33–0.66), respectively against the prior run.

Regarding absolute error metrics (i.e., RMSE), SC3 clearly outperformed both the prior and SC2. Although the absolute differences in RMSE between SC1 and SC3 were relatively small (Table 1), joint assimilation still provided meaningful improvements at several sites, including EASTB, GISBN, MOORH, SOURH and PORTN. Moreover, SC3 required smaller adjustments to hydraulic parameters compared to SC1, suggesting that incorporating initial state information helped moderate parameter updates and led to a more constrained and potentially more physically plausible calibration.

Soil characteristics have a strong influence on JULES performance. Cosby PTFs are calibrated for mineral soils, meaning the JULES model performs well in 'typical mineral soil' but tends to show more errors in areas with high organic content. Prior model results demonstrate this pattern, with an average KGE of 0.34 for 'typical mineral soil' sites and 0.25 for 'high organic content' sites. However, assimilation results (SC3) showed maximum improvement at sites where JULES initially performed poorly. For instance, three of the top four improvements were seen at sites with high organic content: GISBN, CHOBH and MOORH showed improvements of approximately 350%, 250% and 220%, respectively, in KGE values. The post-assimilation model with updated PTF constants and initial conditions performed well across various soil types within the UK, suggesting that this framework has strong potential for broader application.

During state-only assimilation (SC2), the posterior JULES model performed marginally better than the prior run, with a mean improvement of 6% in KGE and 37.1% in RMSE. However, the effect of the updated initial soil moisture condition decayed quickly in less than 6 months. For a few sites, the prior and posterior soil moisture time series coincided within 3 months from the point of assimilation. This limitation can be addressed by assimilating more frequently using a smaller time window. Having a longer time window of 1 year for parameter estimation and multiple shorter time windows of 3 months for state assimilation using a cycling data assimilation system could potentially yield better forecasts.

An important consideration is the relationship between DA and physics-based model development. DA approaches such as the one presented here are not intended to replace physically-based model improvements. On the contrary, insights gained from DA experiments can help diagnose model deficiencies and drive model development. For example, in SC1 and SC3, the changes to the Cosby PTF constants may partly reflect the fact that we are optimising against field-scale COSMOS-UK observations (~12 ha footprint), whereas the original Cosby constants were derived from laboratory analyses of small soil samples (Cosby et al. 1984). This raises questions about whether the physical relationships embedded in JULES hold at the spatial scales at which they are applied, an issue that has been recognised as a fundamental challenge for PTFs in LSMs (Weber et al. 2024). Exploring alternative PTFs, such as the Tóth formulation used by Pinnington et al. (2021), or updated hydraulic parameterisations could provide complementary insights. Similarly, Douglas

14698080, 2026, 5, Downloaded from https://rmets.onlinelibrary.wiley.com/doi/10.1002/met.70256 by UK Centre For Ecology & Hydrology, Wiley Online Library on [19/10/2026]. See the Terms and Conditions (https://onlinelibrary.wiley.com/terms-and-conditions) on Wiley Online Library for rules of use; OA articles are governed by the applicable Creative Commons License

et al. (2025) demonstrated that regularisation of the 4DEnVar can improve the parameter estimation by limiting overfitting, offering a methodological refinement that could be applied within this framework. Such physically-based developments and methodological refinements are beyond the scope of this study but are an important avenue for future work.

It should also be noted that discrepancies between modelled and observed soil moisture may stem from uncertainty in evapotranspiration, which in JULES is calculated using the Penman-Monteith formulation. As independent site observations (e.g., from lysimeters or flux towers) were not available at these sites, incorporating such data offers scope for future work to further constrain soil moisture estimates.

5 | Conclusions

In this study, we presented the first application of joint state-parameter assimilation for the JULES model, allowing both the initial soil moisture conditions and Cosby PTF constants to be optimised simultaneously. Using daily COSMOS-UK observations for 2017 across 16 UK sites, we employed the En-Var hybrid assimilation technique to compare three scenarios: parameter-only (SC1), state-only (SC2) and joint state-parameter (SC3) assimilation. Results demonstrated that jointly updating both the PTF constants and initial soil moisture state consistently outperformed individual scenarios in predicting the soil moisture estimates across the majority of sites and evaluation metrics.

These findings have far-reaching implications beyond the land surface. Soil moisture governs infiltration and runoff generation, directly influencing the magnitude and timing of river flows. Improved soil moisture conditions in JULES can therefore strengthen hydrological forecasting capabilities. As operational weather prediction systems increasingly rely on land surface models like JULES for initialisation, the joint state-parameter framework presented here offers a practical pathway to improve land–atmosphere coupling and land-surface reanalysis. In addition, this work provides a foundation for extending joint assimilation to broader regions and diverse soil types, contributing to disaster preparedness at larger scales.

Author Contributions

Ramesh Visweshwaran: conceptualization, methodology, software, validation, investigation, visualization, writing – original draft, formal analysis, data curation. **Elizabeth Cooper:** software, conceptualization, methodology, validation, investigation, visualization, writing – review and editing, supervision, resources, data curation. **Sarah L. Dance:** conceptualization, methodology, investigation, funding acquisition, writing – review and editing, project administration, supervision, resources, visualization.

Acknowledgments

This work was jointly supported by the Natural Environment Research Council's (NERC) HydroJULES-NEXT project (grant number: NE/X019063/1) and the NERC Climate Change in the Arctic-North Atlantic Region and Impacts on the UK (CANARI) project, (grant number: NE/W004984/1) as a part of the National capability funding programmes. The authors gratefully acknowledge the provision by UKCEH of hydrometeorological and soil data collected by the COSMOS-UK project. COSMOS-UK is funded by the NERC (award no. NE/R016429/1) as part of the UK-SCAPE programme.

Funding

This work was supported by the Natural Environment Research Council (NERC) HydroJULES-NEXT project, Grant/Award Number: NE/X019063/1; NERC Climate Change in the Arctic-North Atlantic Region and Impacts on the UK (CANARI) project, Grant/Award Number: NE/W004984/1.

Conflicts of Interest

The authors declare no conflicts of interest.

Data Availability Statement

JULES source code and the assimilation code used in this study are available from the MetOffice JULES repository (https://code.metoffice.gov.uk/trac/jules, last access: 30 August 2025) under Rose suite number u-dc794. Registration is required. COSMOS-UK data are deposited annually in the NERC Environmental Information Data Centre (EIDC) (https://doi.org/10.5285/b5c190e4-e35d-40ea-8fbe-598da03a1185, Stanley et al. 2021).

References

Albergel, C., P. de Rosnay, G. Balsamo, L. Isaksen, and J. Muñoz-Sabater. 2012. "Soil Moisture Analyses at ECMWF: Evaluation Using Global Ground-Based In Situ Observations." *Journal of Hydrometeorology* 13, no. 5: 1442–1460.

Alvarado-Montero, R., D. Schwanenberg, P. Krahe, P. Helmke, and B. Klein. 2017. "Multi-Parametric Variational Data Assimilation for Hydrological Forecasting." *Advances in Water Resources* 110: 182–192.

Antoniou, V., A. Askquith-Ellis, S. Bagnoli, et al. n.d. "COSMOS-UK User Guide: Users' Guide to Sites, Instruments and Available Data (Version 2.10)."

Best, M. J., M. Pryor, D. B. Clark, et al. 2011. "The Joint UK Land Environment Simulator (JULES), Model Description - Part 1: Energy and Water Fluxes." *Geoscientific Model Development* 4, no. 3: 677–699.

Beven, K., and A. Binley. 1992. "The Future of Distributed Models: Model Calibration and Uncertainty Prediction." *Hydrological Processes* 6, no. 3: 279–298.

Brocca, L., L. Ciabatta, C. Massari, S. Camici, and A. Tarpanelli. 2017. "Soil Moisture for Hydrological Applications: Open Questions and New Opportunities." *Water* 9, no. 2: 140.

Brooks, R. H., and A. T. Corey. n.d. "Hydraulic Properties of Porous Media." Hydrological Papers 3.

Chen, W., C. Huang, H. Shen, and X. Li. 2015. "Comparison of Ensemble-Based State and Parameter Estimation Methods for Soil Moisture Data Assimilation." *Advances in Water Resources* 86: 425–438.

Cooper, E., E. Blyth, H. Cooper, R. Ellis, E. Pinnington, and S. J. Dadson. 2021. "Using Data Assimilation to Optimize Pedotransfer Functions Using Field-Scale in Situ Soil Moisture Observations." *Hydrology and Earth System Sciences* 25, no. 5: 2445–2458.

Cooper, E. S., S. L. Dance, J. García-Pintado, N. K. Nichols, and P. J. Smith. 2019. "Observation Operators for Assimilation of Satellite Observations in Fluvial Inundation Forecasting." *Hydrology and Earth System Sciences* 23, no. 6: 2541–2559.

Cooper, H. M., E. Bennett, J. Blake, et al. 2021. "COSMOS-UK: National Soil Moisture and Hydrometeorology Data for Environmental Science Research." *Earth System Science Data* 13, no. 4: 1737–1757.

14698080, 2026, 5, Downloaded from https://rmets.onlinelibrary.wiley.com/doi/10.1002/met.70256 by UK Centre For Ecology & Hydrology, Wiley Online Library on [19/10/2026]. See the Terms and Conditions (https://onlinelibrary.wiley.com/terms-and-conditions) on Wiley Online Library for rules of use; OA articles are governed by the applicable Creative Commons License

Cosby, B. J., G. M. Hornberger, R. B. Clapp, and T. R. Ginn. 1984. "A Statistical Exploration of the Relationships of Soil Moisture Characteristics to the Physical Properties of Soils." *Water Resources Research* 20, no. 6: 682–690.

Douglas, N., S. Beylat, T. Quaife, P. Peylin, N. Raoult, and R. Bannister. 2026. "Regularisation of the 4DEnVar Data Assimilation Method for Calibration of Land Surface Models." *EGUsphere* 2026: 1–25.

Douglas, N., T. Quaife, and R. Bannister. 2025. "Exploring a Hybrid Ensemble–Variational Data Assimilation Technique (4DEnVar) With a Simple Ecosystem Carbon Model." *Environmental Modelling & Software* 186: 106361.

Dumedah, G., and J. P. Walker. 2014. "Intercomparison of the JULES and CABLE Land Surface Models Through Assimilation of Remotely Sensed Soil Moisture in Southeast Australia." *Advances in Water Resources* 74: 231–244.

Entekhabi, D., E. G. Njoku, P. E. O'Neill, et al. 2010. "The Soil Moisture Active Passive (SMAP) Mission." *Proceedings of the IEEE* 98, no. 5: 704–716.

Evans, J. G., H. C. Ward, J. R. Blake, et al. 2016. "Soil Water Content in Southern England Derived From a Cosmic-Ray Soil Moisture Observing System – COSMOS-UK." *Hydrological Processes* 30, no. 26: 4987–4999.

Fischer, G., F. Nachtergaele, S. Prieler, H. Van Velthuizen, L. Verelst, and D. Wiberg. n.d. "Harmonized-World-Soil-Database-v12." Global Agro-Ecological Zones Assessment for Agriculture (GAEZ 2008), IIASA, Laxenburg, Austria and FAO, Rome, Italy, 10.

Gong, J., X. Liu, C. Yao, et al. 2024. "State Updating in the Xin'anjiang Model: Joint Assimilating Streamflow and Multi-Source Soil Moisture Data via Asynchronous Ensemble Kalman Filter With Enhanced Error Models." *Hydrology and Earth System Sciences Discussions* 2024: 1–38.

Gupta, H. V., H. Kling, K. K. Yilmaz, and G. F. Martinez. 2009. "Decomposition of the Mean Squared Error and NSE Performance Criteria: Implications for Improving Hydrological Modelling." *Journal of Hydrology* 377, no. 1: 80–91.

Han, X., H.-J. H. Franssen, C. Montzka, and H. Vereecken. 2014. "Soil Moisture and Soil Properties Estimation in the Community Land Model With Synthetic Brightness Temperature Observations." *Water Resources Research* 50, no. 7: 6081–6105.

Heyvaert, Z., S. Scherrer, W. Dorigo, M. Bechtold, and G. De Lannoy. 2024. "Joint Assimilation of Satellite-Based Surface Soil Moisture and Vegetation Conditions Into the Noah-MP Land Surface Model." *Science of Remote Sensing* 9: 100129.

Hou, Z., and Z. Pu. 2023. "Assessing CYGNSS Satellite Soil Moisture Data for Drought Monitoring With Multiple Datasets and Indicators." *Remote Sensing* 16, no. 1: 116.

Huggannavar, V., and J. Indu. 2020. "Seasonal Variability of Soil Moisture-Precipitation Feedbacks Over India." *Journal of Hydrology* 589: 125181.

Janjić, T., N. Bormann, M. Bocquet, et al. 2018. "On the Representation Error in Data Assimilation." *Quarterly Journal of the Royal Meteorological Society* 144, no. 713: 1257–1278.

Kerr, Y. H., P. Waldteufel, J.-P. Wigneron, J. Martinuzzi, J. Font, and M. Berger. 2001. "Soil Moisture Retrieval From Space: The Soil Moisture and Ocean Salinity (SMOS) Mission." *IEEE Transactions on Geoscience and Remote Sensing* 39, no. 8: 1729–1735.

Kumar, S., J. Kolassa, R. Reichle, et al. 2022. "An Agenda for Land Data Assimilation Priorities: Realizing the Promise of Terrestrial Water, Energy, and Vegetation Observations From Space." *Journal of Advances in Modeling Earth Systems* 14, no. 11: e2022MS003259.

Liu, Z.-Q., and F. Rabier. 2003. "The Potential of High-Density Observations for Numerical Weather Prediction: A Study With Simulated Observations." *Quarterly Journal of the Royal Meteorological Society* 129, no. 594: 3013–3035.

Lorenc, A. C., N. E. Bowler, A. M. Clayton, S. R. Pring, and D. Fairbairn. 2015. "Comparison of Hybrid-4DEnVar and Hybrid-4DVar Data Assimilation Methods for Global NWP." *Monthly Weather Review* 143, no. 1: 212–229.

Lü, H., Z. Yu, Y. Zhu, S. Drake, Z. Hao, and E. A. Sudicky. 2011. "Dual State-Parameter Estimation of Root Zone Soil Moisture by Optimal Parameter Estimation and Extended Kalman Filter Data Assimilation." *Advances in Water Resources* 34, no. 3: 395–406.

Mahfouf, J.-F., and P. Viterbo. 1996. "Land Surface Assimilation." In *Proceedings of the Seminar on Data Assimilation*, vol. 319, 347. ECMWF (European Centre for Medium-Range Weather Forecasts).

Marthews, T. R., C. A. Quesada, D. R. Galbraith, et al. 2014. "High-Resolution Hydraulic Parameter Maps for Surface Soils in Tropical South America." *Geoscientific Model Development* 7, no. 3: 711–723.

Martínez-de la Torre, A., E. M. Blyth, and G. P. Weedon. 2019. "Using Observed River Flow Data to Improve the Hydrological Functioning of the JULES Land Surface Model (vn4.3) Used for Regional Coupled Modelling in Great Britain (UKC2)." *Geoscientific Model Development* 12, no. 2: 765–784.

Mason, D., J. Garcia-Pintado, H. Cloke, S. Dance, and J. Munoz-Sabater. 2020. "Assimilating High Resolution Remotely Sensed Soil Moisture Into a Distributed Hydrologic Model to Improve Runoff Prediction."

Muñoz Sabater, J., E. Dutra, A. Agustí-Panareda, et al. 2021. "ERA5-Land: A State-of-the-Art Global Reanalysis Dataset for Land Applications." *Earth System Science Data* 13, no. 9: 4349–4383.

Nearing, G., S. Yatheendradas, W. Crow, X. Zhan, J. Liu, and F. Chen. 2018. "The Efficiency of Data Assimilation." *Water Resources Research* 54, no. 9: 6374–6392.

Pinnington, E., J. Amezcua, E. Cooper, et al. 2021. "Improving Soil Moisture Prediction of a High-Resolution Land Surface Model by Parameterising Pedotransfer Functions Through Assimilation of SMAP Satellite Data." *Hydrology and Earth System Sciences* 25, no. 3: 1617–1641.

Pinnington, E., T. Quaife, A. Lawless, K. Williams, T. Arkebauer, and D. Scoby. 2020. "The Land Variational Ensemble Data Assimilation Framework: LAVENDAR v1.0.0." *Geoscientific Model Development* 13, no. 1: 55–69.

Pinnington, E. M., E. Casella, S. L. Dance, et al. 2017. "Understanding the Effect of Disturbance From Selective Felling on the Carbon Dynamics of a Managed Woodland by Combining Observations With Model Predictions." *Journal of Geophysical Research: Biogeosciences* 122, no. 4: 886–902.

Poterjoy, J., and F. Zhang. 2015. "Systematic Comparison of Four-Dimensional Data Assimilation Methods With and Without the Tangent Linear Model Using Hybrid Background Error Covariance: E4DVar Versus 4DEnVar." *Monthly Weather Review* 143, no. 5: 1601–1621.

Ramesh, V., A. Patil, and R. A. A. J. Ramsankaran. 2025. "Dual Correction of Rainfall and Root Zone Soil Moisture Estimates for Improving Streamflow Simulations." *ARC Geophysical Research* 1, no. 1.

Raoult, N., N. Douglas, N. MacBean, et al. 2025. "Parameter Estimation in Land Surface Models: Challenges and Opportunities With Data Assimilation and Machine Learning." *Journal of Advances in Modeling Earth Systems* 17, no. 11: e2024MS004733.

Ridler, M.-E., H. Madsen, S. Stisen, S. Bircher, and R. Fensholt. 2014. "Assimilation of SMOS-Derived Soil Moisture in a Fully Integrated Hydrological and Soil-Vegetation-Atmosphere Transfer Model in Western Denmark." *Water Resources Research* 50, no. 11: 8962–8981.

Ritchie, P. D. L., A. B. Harper, G. S. Smith, et al. 2019. "Large Changes in Great Britain's Vegetation and Agricultural Land-Use Predicted Under

14698080, 2026, 5, Downloaded from https://rmets.onlinelibrary.wiley.com/doi/10.1002/met.70256 by UK Centre For Ecology & Hydrology, Wiley Online Library on [19/10/2026]. See the Terms and Conditions (https://onlinelibrary.wiley.com/terms-and-conditions) on Wiley Online Library for rules of use; OA articles are governed by the applicable Creative Commons License

Unmitigated Climate Change." *Environmental Research Letters* 14, no. 11: 114012.

Seo, E., M.-I. Lee, and R. H. Reichle. 2021. "Assimilation of SMAP and ASCAT Soil Moisture Retrievals Into the JULES Land Surface Model Using the Local Ensemble Transform Kalman Filter." *Remote Sensing of Environment* 253: 112222.

Shi, Y., K. J. Davis, F. Zhang, C. J. Duffy, and X. Yu. 2015. "Parameter Estimation of a Physically-Based Land Surface Hydrologic Model Using an Ensemble Kalman Filter: A Multivariate Real-Data Experiment." *Advances in Water Resources* 83: 421–427.

Smith, P. J., G. D. Thornhill, S. L. Dance, A. S. Lawless, D. C. Mason, and N. K. Nichols. 2013. "Data Assimilation for State and Parameter Estimation: Application to Morphodynamic Modelling." *Quarterly Journal of the Royal Meteorological Society* 139, no. 671: 314–327.

Stanley, S., V. Antoniou, and A. Askquith-Ellis. 2021. "Daily and sub-daily Hydrometeorological and Soil Data (2013-2019) [COSMOS-UK]." *NERC Environmental Information Data Centre*. https://doi.org/10.5285/b5c190e4-e35d-40ea-8fbe-598da03a1185.

Stanley, S., V. Antoniou, A. Askquith-Ellis, et al. 2023. "Daily and Sub-Daily Hydrometeorological and Soil Data (2013–2022) [COSMOS-UK]."

Stewart, L. M., S. L. Dance, and N. K. Nichols. 2008. "Correlated Observation Errors in Data Assimilation." *International Journal for Numerical Methods in Fluids* 56, no. 8: 1521–1527.

Subbarayan, S., Y. M. Youssef, L. Singh, et al. 2025. "Soil and Water Assessment Tool-Based Prediction of Runoff Under Scenarios of Land Use/Land Cover and Climate Change Across Indian Agro-Climatic Zones: Implications for Sustainable Development Goals." *Water* 17, no. 3: 458. https://doi.org/10.3390/w17030458.

Sumargo, E., H. McMillan, R. Weihs, C. J. Ellis, A. M. Wilson, and F. M. Ralph. 2021. "A Soil Moisture Monitoring Network to Assess Controls on Runoff Generation During Atmospheric River Events." *Hydrological Processes* 35, no. 1: e13998.

Tian, S., L. J. Renzullo, R. C. Pipunic, J. Lerat, W. Sharples, and C. Donnelly. 2021. "Satellite Soil Moisture Data Assimilation for Improved Operational Continental Water Balance Prediction." *Hydrology and Earth System Sciences* 25, no. 8: 4567–4584.

Tóth, B., M. Weynants, A. Nemes, A. Makó, G. Bilas, and G. Tóth. 2015. "New Generation of Hydraulic Pedotransfer Functions for Europe." *European Journal of Soil Science* 66, no. 1: 226–238.

van Genuchten, M. T. 1980. "A Closed-Form Equation for Predicting the Hydraulic Conductivity of Unsaturated Soils." *Soil Science Society of America Journal* 44, no. 5: 892–898.

Van Looy, K., J. Bouma, M. Herbst, et al. 2017. "Pedotransfer Functions in Earth System Science: Challenges and Perspectives." *Reviews of Geophysics* 55, no. 4: 1199–1256.

Visweshwaran, R., R. A. A. J. Ramsankaran, and T. I. Eldho. 2024. "Improving Modelled Streamflow Using Time-Varying Multivariate Assimilation of Remotely Sensed Soil Moisture and In-Situ Streamflow Observations." *Advances in Water Resources* 186: 104676.

Visweshwaran, R., R. A. A. J. Ramsankaran, T. I. Eldho, and M. K. Jha. 2022. "Hydrological Impact Assessment of Future Climate Change on a Complex River Basin of Western Ghats, India." *Water* 14, no. 21: 3571. https://doi.org/10.3390/w14213571.

Visweshwaran, R., R. A. A. J. Ramsankaran, T. I. Eldho, and S. Lakshmivarahan. 2022. "Sensitivity-Based Soil Moisture Assimilation for Improved Streamflow Forecast Using a Novel Forward Sensitivity Method (FSM) Approach." *Water Resources Research* 58, no. 1: e2021WR031092.

Wagner, W., S. Hahn, R. Kidd, et al. 2013. "The ASCAT Soil Moisture Product: A Review of Its Specifications, Validation Results, and Emerging Applications." *Meteorologische Zeitschrift* 22, no. 1: 5–33.

Walker, J. P., and P. R. Houser. 2001. "A Methodology for Initializing Soil Moisture in a Global Climate Model: Assimilation of Near-Surface Soil Moisture Observations." *Journal of Geophysical Research: Atmospheres* 106, no. D11: 11761–11774.

Weber, T. K. D., L. Weihermüller, A. Nemes, et al. 2024. "Hydro-Pedotransfer Functions: A Roadmap for Future Development." *Hydrology and Earth System Sciences* 28, no. 14: 3391–3433.

Wigneron, J.-P., S. Dayan, A. Kruszewski, et al. 2018. "The Aqui Network: Soil Moisture Sites in the 'Les Landes' Forest and Graves Vineyards (Bordeaux Aquitaine Region, France)." In *IGARSS 2018–2018 IEEE International Geoscience and Remote Sensing Symposium*, 3739–3742. IEEE.

Xaver, A., L. Zappa, G. Rab, et al. 2020. "Evaluating the Suitability of the Consumer Low-Cost Parrot Flower Power Soil Moisture Sensor for Scientific Environmental Applications." *Geoscientific Instrumentation, Methods and Data Systems* 9, no. 1: 117–139.

Xu, Y., J.-C. Calvet, and B. Bonan. 2025. "The Joint Assimilation of Satellite Observed LAI and Soil Moisture for the Global Root Zone Soil Moisture Production and Its Impact on Land Surface and Ecosystem Variables." *Agricultural and Forest Meteorology* 360: 110299.

Zha, Y., P. Zhu, Q. Zhang, W. Mao, and L. Shi. 2019. "Investigation of Data Assimilation Methods for Soil Parameter Estimation With Different Types of Data." *Vadose Zone Journal* 18, no. 1: 190013.

14698080, 2026, 5, Downloaded from https://rmets.onlinelibrary.wiley.com/doi/10.1002/met.70256 by UK Centre For Ecology & Hydrology, Wiley Online Library on [19/10/2026]. See the Terms and Conditions (https://onlinelibrary.wiley.com/terms-and-conditions) on Wiley Online Library for rules of use; OA articles are governed by the applicable Creative Commons License

Appendix A

Updated JULES Initial Soil Moisture Condition During State-Parameter Scenario

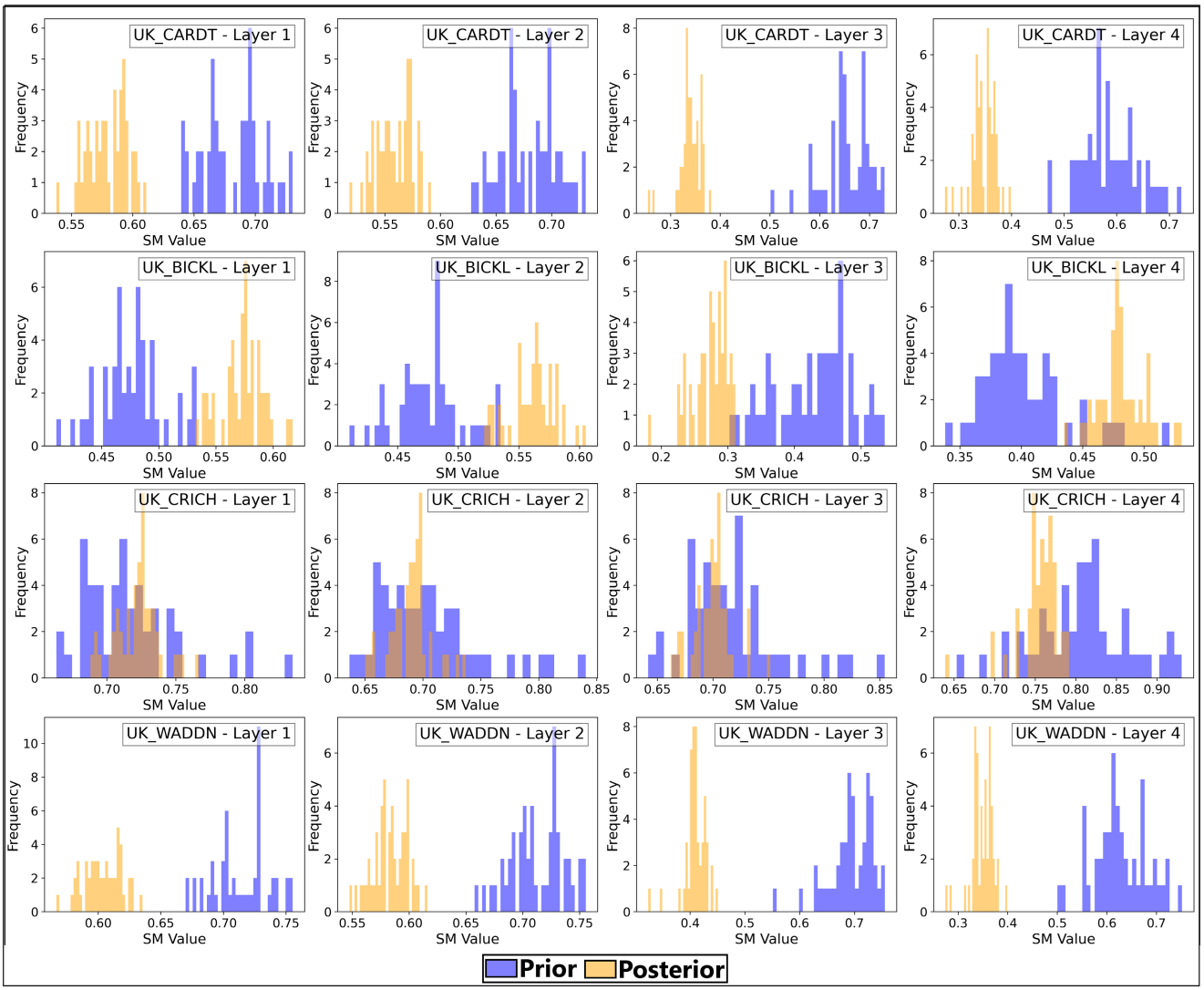


FIGURE A1 | Prior and posterior distribution values of JULES's initial soil moisture condition at CARDT, BICKL, CRICH and WADDN COSMOS-UK sites during state-parameter assimilation.

14698080, 2026, 5, Downloaded from https://rmets.onlinelibrary.wiley.com/doi/10.1002/met.70256 by UK Centre For Ecology & Hydrology, Wiley Online Library on [19/10/2026]. See the Terms and Conditions (https://onlinelibrary.wiley.com/terms-and-conditions) on Wiley Online Library for rules of use; OA articles are governed by the applicable Creative Commons License

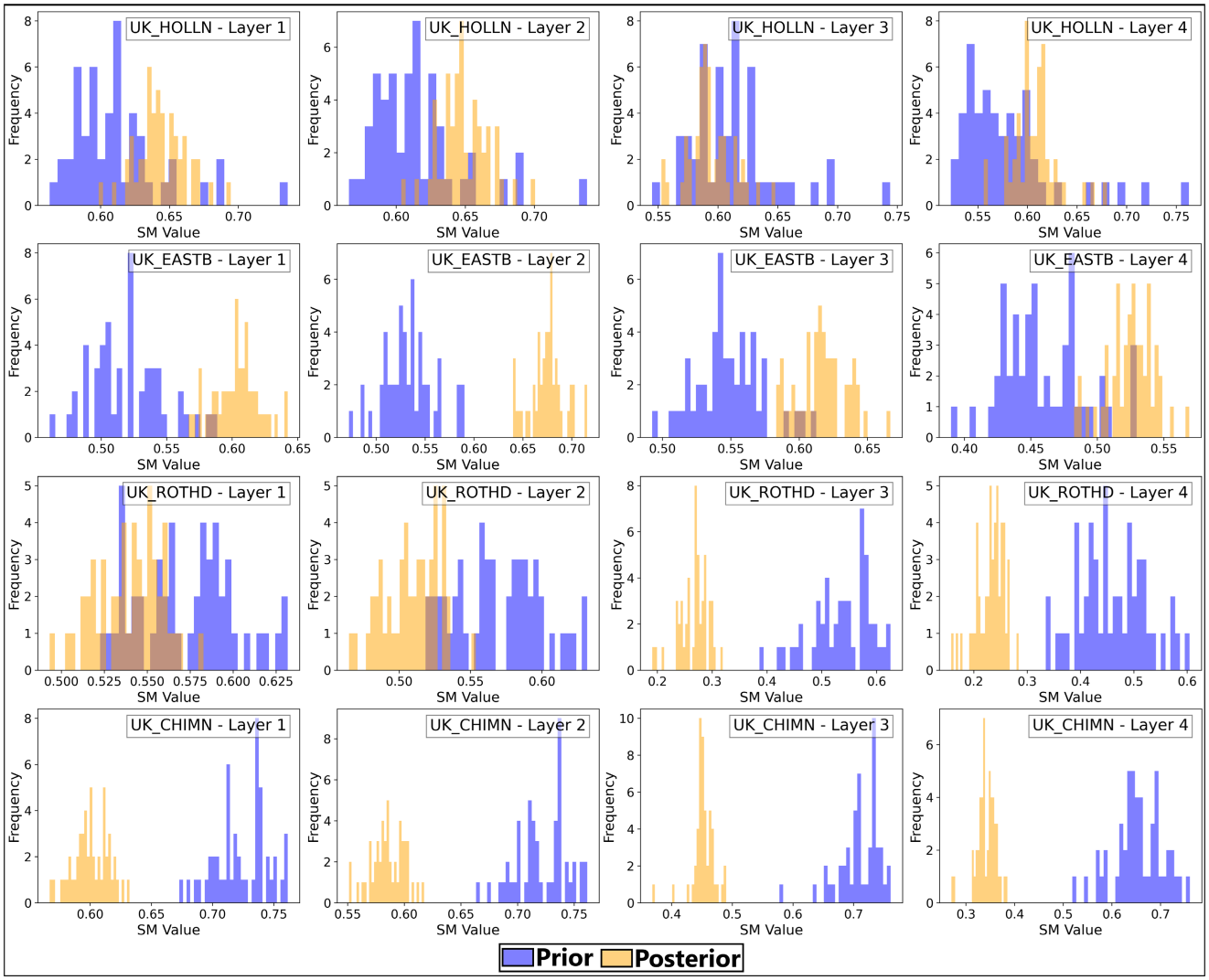


FIGURE A2 | Prior and posterior distribution values of JULES's initial soil moisture condition at HOLLN, EASTB, ROTHD and CHIMN COSMOS-UK sites during state-parameter assimilation.

14698080, 2026, 5, Downloaded from https://rmets.onlinelibrary.wiley.com/doi/10.1002/met.70256 by UK Centre For Ecology & Hydrology, Wiley Online Library on [19/10/2026]. See the Terms and Conditions (https://onlinelibrary.wiley.com/terms-and-conditions) on Wiley Online Library for rules of use; OA articles are governed by the applicable Creative Commons License

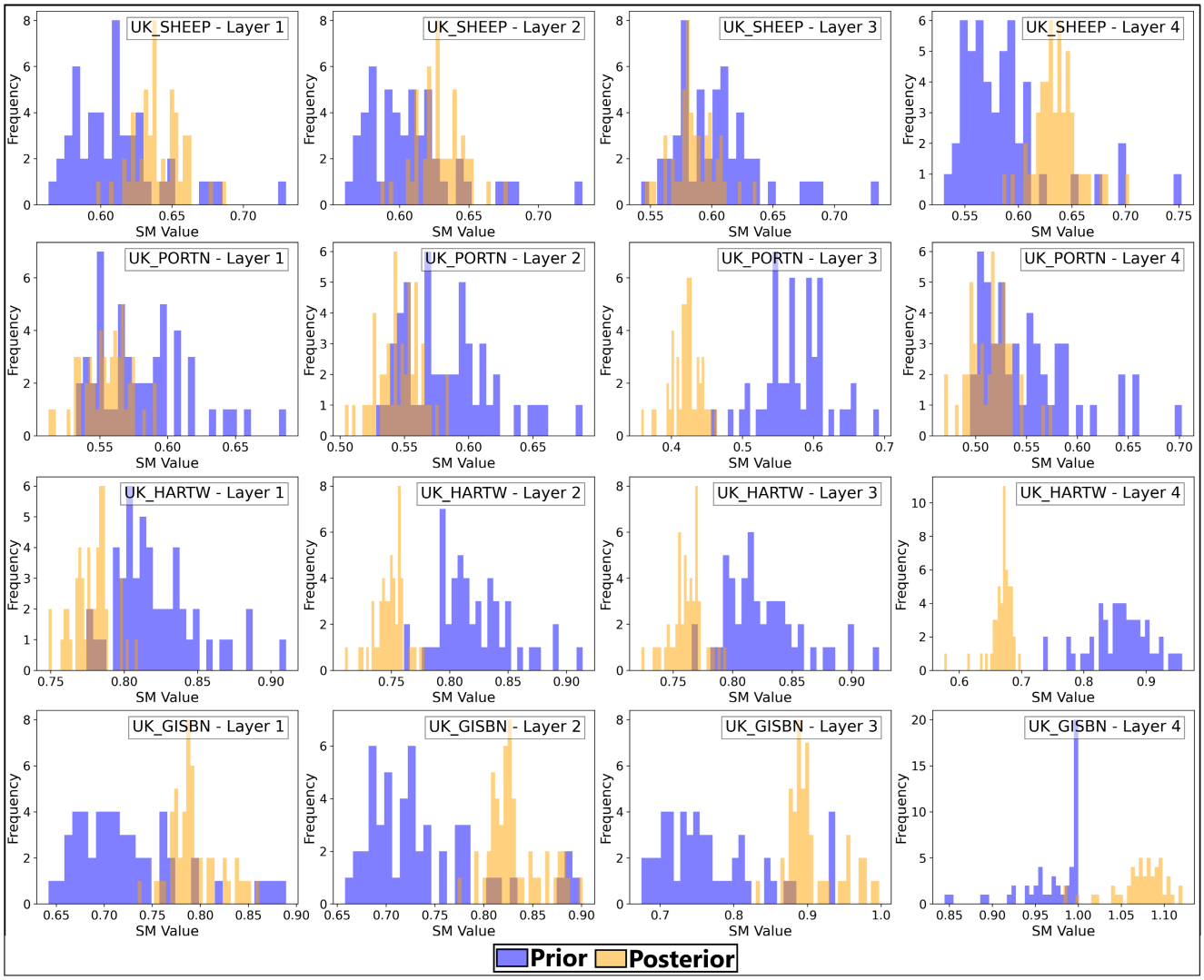


FIGURE A3 | Prior and posterior distribution values of JULES's initial soil moisture condition at SHEEP, PORTN, HARTW and GISBN COSMOS-UK sites during state-parameter assimilation.

14698080, 2026, 5, Downloaded from https://rmets.onlinelibrary.wiley.com/doi/10.1002/met.70256 by UK Centre For Ecology & Hydrology, Wiley Online Library on [19/10/2026]. See the Terms and Conditions (https://onlinelibrary.wiley.com/terms-and-conditions) on Wiley Online Library for rules of use; OA articles are governed by the applicable Creative Commons License

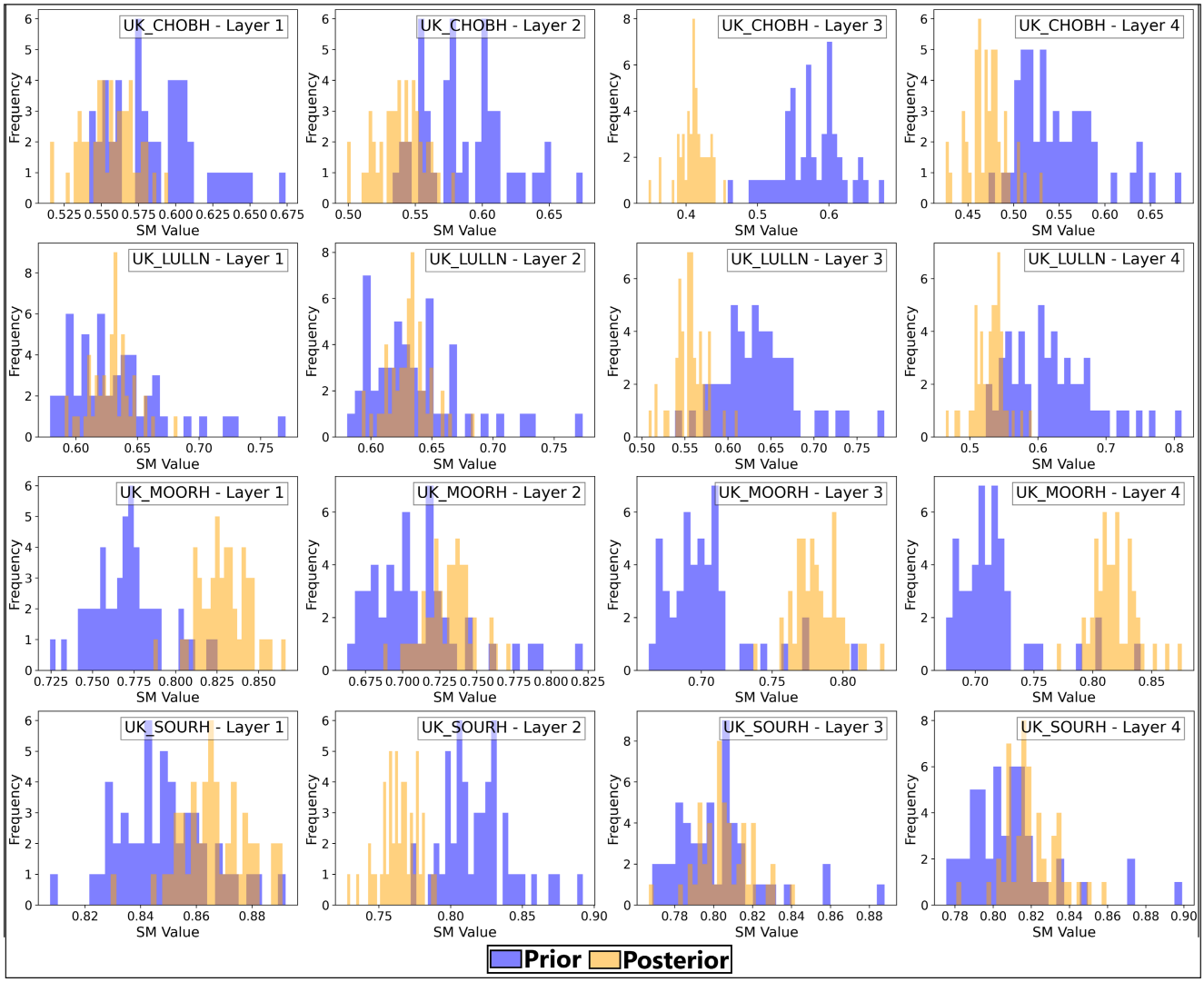


FIGURE A4 | Prior and posterior distribution values of JULES's initial soil moisture condition at CHOBH, LULLN, MOORH and SOURH COSMOS-UK sites during state-parameter assimilation.

14698080, 2026, 5, Downloaded from https://rmets.onlinelibrary.wiley.com/doi/10.1002/met.70256 by UK Centre For Ecology & Hydrology, Wiley Online Library on [19/10/2026]. See the Terms and Conditions (https://onlinelibrary.wiley.com/terms-and-conditions) on Wiley Online Library for rules of use; OA articles are governed by the applicable Creative Commons License